HHS Public Access

Author manuscript

J Dev Orig Health Dis. Author manuscript; available in PMC 2021 October 01.

Published in final edited form as:

J Dev Orig Health Dis. 2021 April ; 12(2): 203–219. doi:10.1017/S2040174420001233.

Cardiac magnetic resonance imaging: insights into developmental programming and its consequences for aging

G.D. Clarke[1,2], **J. Li**[1,2], **A.H. Kuo**[3], **A.J. Moody**[1,2], **P.W. Nathanielsz**[4]

[1]Department of Radiology, University of Texas Health Science Center at San Antonio, San Antonio, TX, USA

[2]Research Imaging Institute, University of Texas Health Science Center at San Antonio, San Antonio, TX, USA

[3]Department of Radiology, Massachusetts General Hospital, Boston, MA, USA

[4]Department of Animal Science, University of Wyoming, Laramie, WY, USA

Abstract

Cardiovascular diseases (CVD) are important consequences of adverse perinatal conditions such as fetal hypoxia and maternal malnutrition. Cardiac magnetic resonance imaging (CMR) can produce a wealth of physiological information related to the development of the heart. This review outlines the current state of CMR technologies and describes the physiological biomarkers that can be measured. These phenotypes include impaired ventricular and atrial function, maladaptive ventricular remodeling, and the proliferation of myocardial steatosis and fibrosis. The discussion outlines the applications of CMR to understanding the developmental pathways leading to impaired cardiac function. The use of CMR, both in animal models of developmental programming and in human studies, is described. Specific examples are given in a baboon model of intrauterine growth restriction (IUGR). CMR offers great potential as a tool for understanding the sequence of dysfunctional adaptations of developmental origin that can affect the human cardiovascular system.

Keywords

Heart disease; cardiac MRI; ventricular remodeling; developmental programming

DOHaD and heart disease

Cardiovascular disease (CVD) plays a major role in the genesis of human morbidity and mortality. Some of the earliest clues that early life stresses can predispose to severe health consequences in later life were the links found between perinatal dietary challenges imposed by war and famine and the increased risk for chronic later life CVD.[1] Further human

Address for correspondence: GD Clarke, Department of Radiology, University of Texas Health Science Center at San Antonio and Research Imaging Institute, University of Texas Health Science Center at San Antonio and Research Imaging Institute, University of Texas Health Science Center at San Antonio, San Antonio, TX, USA. CLARKEG@uthscsa.edu.

Conflicts of interest. The authors have no potential conflict of interest, financial or otherwise, to disclose.

epidemiological studies and carefully controlled animal experiments established that both maternal nutrient restriction (MNR) and overnutrition predispose offspring to an increased prevalence of obesity, glucose intolerance, insulin resistance, endocrine and renal dysfunction, hypertension, and vascular dysfunction as well as heart disease that varies with the precise timing of the nutritional challenge.[2] These same insights have been reported in a variety of studies conducted in multiple countries over the last two decades.[3,4]

The study of the developmental origins of health and disease focusses on the process of "developmental programming", which aims to discover mechanisms that underlie adaptations to a poor nutritional environment and other challenges occurring during development. The premise is that responses to developmental challenges can enhance short-term survival outcomes, but in so doing alter the trajectory of development in many physiological systems (metabolic, cardiac, renal, neural, and reproductive). Consequently, programming predisposes an individual to be more susceptible to chronic diseases later in life.

During development, a series of epigenetic processes are central to normal fetal development. *In utero* challenges to the fetus such as nutrient restriction, fetal hypoxia due to placental insufficiency, anemia, maternal obesity, and overnutrition, respiratory disease, and/or preeclampsia elicit physiological adaptations aimed at overcoming nutrient deficiencies in order to maintain fetal viability.[5,6] These challenges begin a process that includes other epigenetic changes that can predispose the offspring to CVD in later life.[7] Key myocardial biomarkers resulting from these processes are ventricular remodeling and cardiac fibrosis.[8] More recently, the life course consequences of exposure to perinatal environmental toxins due to maternal smoking, pollution, alcohol, and consumption of drugs of abuse have increased the scope of intensive programming investigations.[9,10]

Epidemiological studies typically employ public medical databases and focus on diagnostic end points. This approach provides powerful distribution patterns, but lacks the ability to determine causative mechanisms by which malnutrition and other early challenges alter the physiology of maturation, life course disease pathology, and aging. Mechanistic pathways are best obtained in carefully controlled experiments studying appropriate animal models of fetal programming.

Application of classical physiological and molecular biological methods has improved specific understanding of the potential mechanisms involved in the developmental programming of CVD. For example, the expressions of cardiac-specific transcription factors have been shown to be disrupted during fetal development affecting the renin–angiotensin system (RAS).[11] Altered expressions of angiotensin II type 1 and type 2 occur with perinatal hypoxia in many species, which result in impaired kidney development and lead to hypertension in adult life.[12] Histone deacetylases have been shown to play complicated roles in cardiomyocyte development and are implicated in the programming of endothelial dysfunction.[13] Also, sex-dependent accumulation of fibrotic tissue, activation of cardiac autophagy, and myocardial miRNAs were found in fetuses of baboons with calorie-restricted diets during pregnancy.[14] Changes in cardiac miRNA also have been demonstrated in the response to maternal obesity and high-fat diets.[15] The degree to which each of these factors,

and many others affecting multiple systems, combine to determine the phenotype of the programmed heart is still incompletely understood despite abundant knowledge of individual mechanisms.

In this review, we discuss the use of noninvasive cardiac magnetic resonance imaging (CMR) to evaluate developmental programming in both human cohorts and animal models with a spotlight on its ability to assess cardiovascular physiology. Although ultrasound has been widely used in obstetrical research, here we focus on CMR as an imaging modality that has unique and powerful capabilities to evaluate cardiovascular morphology, physiology, tissue microstructure, and biochemistry. We describe the technical capabilities of CMR, review the research reported to date, and discuss additional applications for potential exploitation of CMR in future studies on the developmental origins of CVD. The following discussion also will explain how CMR can not only produce information on physiological consequences, but also may provide insights into which cell types are susceptible to epigenetic modifications and other alterations relevant to developmental programming.

CVD imaging phenotypes in developmental programming

Until recently, technological limitations did not allow for a detailed understanding of the overall effect of disease progression in complex mammalian organisms. Now, advances in noninvasive quantitative imaging methods applied to whole organisms provide tools and methods for gaining new insights into underlying physiological and pathophysiological processes. For example, the details of atherosclerotic plaque progression were not appreciated until intravascular ultrasound became available in the 1990s, allowing physicians to discern the differences between vulnerable and stable coronary plaques and to appreciate the role of atheromatous plaque remodeling on coronary restenosis.[16] However, intravascular ultrasound is invasive and requires placement under fluoroscopy guidance, which can produce a significant radiation dose.

Ultrasound is a well-established and extensively used tool for obstetric evaluations of fetal and placental health, which can also be used to assess early life course adaptations to fetal stress exposures in humans. In studying developmental programming, echocardiographic investigations of late-onset small fetuses have reported relative increases in left ventricle (LV) sphericity (globular phenotype), LV length (elongated phenotype), and LV myocardial wall thickness (hypertrophic phenotype).[17,18] The hypertrophic phenotype has been attributed to early onset intrauterine growth restriction (IUGR) while the elongated and spherical phenotypes represent degrees of remodeling in late-onset IUGR.[19] Further, fetal M-mode and Doppler echocardiography studies have revealed deficits in both systolic and diastolic function associated with IUGR.[19]

Echocardiography can also reveal CVD progression after birth. A study conducted in neonates deemed small for gestational age (SGA), both prenatally and at 6months, showed a more globular cardiac shape prenatally and as infants compared to controls.[20] In addition, there were signs of systolic longitudinal dysfunction, both prenatally and postnatally, tricuspid annular plane systolic excursion, and diastolic dysfunction. In a separate study, Ponderal index was significantly lower, blood pressure was significantly higher, diastolic

dysfunction was greater, and aortic intima-media thickness was significantly greater in term-born SGA infants compared to controls.[21]

Echocardiography also has been used in small animal models to study the mechanisms of CVD in the setting of fetal programming. High-resolution echocardiography has been used to evaluate the effect of a prenatal hypoxic insult on cardiovascular function in a rat model of IUGR.[22] This study revealed an increased susceptibility to additional stresses, such as myocardial ischemia, for offspring with hypoxia-induced IUGR. The same group studied a placental hypoxia rat model, using echocardiography to demonstrate improved diastolic function in 7-month-old female rat offspring, whose mothers had been treated prenatally with the antioxidant, MitoQ.[23] Administration of a low-protein diet during pregnancy and lactation to Wistar–Kyoto dams was found to reduce aortic peak systolic velocity measured by echocardiography in 18-week-old offspring.[24]

Transthoracic echocardiography is widely employed to assess cardiovascular hemodynamics, yielding physical parameters that are used to characterize blood flow. The success of studies that have used echocardiography to identify CVD imaging phenotypes of developmental programming, in both humans and rodents, implies that there may be applications for other noninvasive imaging technologies with greater levels of sensitivity that can discern additional characteristics related to heart structure and function. Echocardiography is convenient due to its availability, relatively low expense, portability of the equipment, and high temporal resolution. However, the ultrasonic imaging process relies on a sound beam entering and leaving the body through the standard “acoustic windows”, which often necessitates visualizing deep structures from limited perspectives. In addition, studies may have inadequate image quality due to the inability to compensate for respiratory variation and lack of operator skill. Echocardiography also suffers from numerous artifacts that are associated with the physics of sound reflection and refraction in the body, ultrasound beam properties, and/or transceiver electronics.

CMR is equally noninvasive and can generate extensive physiological information about subclinical functional and structural abnormalities of the heart. Like ultrasound, CMR can be used multiple times across the life span of a subject to follow the trajectory of the cardiovascular changes without dangers such as repeated ionizing radiation exposure. However, some patients may not be able to tolerate CMR well, being anxious at confinement in a tube for up to an hour or unable to hold their breath during data acquisition. Patients with arrhythmias or who present challenges in detecting ECG vectors make it difficult to obtain static images at specific times in the cardiac cycle. In conventional cine CMR, magnetic field inhomogeneities can produce black lines that have to be avoided. Also, signal voids in the anterior LV wall can appear due to sternal wires in patients who have had thoracic surgery. Other artifacts that appear include chemical shift artifacts that present as the signal from pericardial fat overlapping the myocardium and ghosting artifacts due to pulsatile flow of blood in the pulmonary arteries and aorta. This article explains the particular advantages of using CMR to evaluate the interrelationships of fetal programming and life course and aging cardiovascular changes.

Cardiac MRI evaluations of heart anatomy, physiology, and biochemistry

Almost four decades after its establishment as an effective clinical diagnostic modality, CMR also is becoming recognized as a research tool that can produce quantitative imaging biomarkers to understand both normal and subtly dysregulated biological processes. CMR is a specialized application of MRI that includes a group of tools that have been developed to assess cardiac function and structure. In particular, CMR can be used to evaluate both rest and stress left ventricular (LV) and right ventricular (RV) function and anatomy, atrial function/anatomy, ventricular stresses and strains, tissue composition, the biochemical environment, pericardial fat deposition, and blood flow within vessels and chambers.

Since the clinical introduction of MRI in the early 1980s, CMR has exhibited the capability to measure important cardiological parameters with great flexibility and high precision. These assessments all are performed *in vivo*, requiring only that the subject stay immobile during scanning, probably having to perform a breath hold during each scan. A few CMR measurements also utilize exogenous contrast agents, which are injected intravenously. In spite of its general acceptance, the scope of utilization of CMR largely has been limited because of instrumentation cost, availability, and the technical skill required to successfully perform quantitative CMR studies and analyses.

It was soon recognized that CMR could produce accurate measurements of LV volume and myocardial mass.[25] However, these early studies covered limited portions of the heart and were not time or cost-efficient. Acquisition of lines of CMR image data are triggered to an ECG signal and are acquired during a series of heartbeats to create an image. The development of breath-hold segmented gradient-echo CMR techniques allowed reduced data acquisition which lowered scan time to 15–20 heartbeats, allowing accurate assessments of LV function.[26] Initially, the motion of a single myocardial slice could be imaged as a cine loop across the R-R interval. With modern hardware and image reconstruction methods, multiple slices and currently, the entire beating heart can be imaged in a single breath hold. Although they are readily visualized on CMR, the papillary muscles and trabecular tissues typically are routinely ignored in measurements of ventricular volume, in order for CMR results to be comparable to those obtained from modalities in which these structures cannot be identified. Being able to measure ventricular volumes at end-diastole (ED) and end-systole (ES) allows for the direct calculation of ejection fraction, stroke volume, and cardiac output (Fig. 1a–f).[27] The ability to measure LV and RV volumes at ~30 ms intervals during a cardiac cycle enables measurements of ventricular ejection rates and ventricular filling rates. Further, the disordered backflow due to regurgitation can be visualized in these cine images as black jets (signal voids) that are a sign of valvular insufficiency.[28] Today, a typical whole-heart cine CMR study typically is 25–30 cardiac phases and 20–25 slices of the heart, comprising a total of 500 or more images.

Determining the functional phenotypes from these image datasets requires delineation of the cardiac boundaries. Performed manually, this is a very time-consuming process, so state-of-the-art techniques incorporating machine learning have been developed for the automatic and semi-automatic segmentation of cardiac structures and calculation of physiological parameters.[29] Several cardiac image analysis software products are available, both

commercial and freely available packages.[30,31] Most of the MRI system manufacturers also offer cardiac post-processing modules. Fig. 1 shows the steps performed for a typical baboon heart segmentation of the RV and LV using the cmr42™ cardiac image analysis software (Circle Cardiovascular Imaging Inc., Alberta, Canada).

One reason for the limited use of CMR is that many clinically important measures can be obtained using other, more established, imaging modalities. Biplanar fluoroscopic X-ray angiography and multi-detector X-ray computed tomography (CT) can both visualize the ventricular lumens and provide model-based estimations of ejection fraction and cardiac output. However, these modalities come with risks to the patient from iodinated contrast agents and ionizing radiation exposures. Radiation risks also may be greater in pediatric patients.[32] Single-photon emission computed tomography (SPECT) can also produce ejection fraction estimates, but also imposes a radiation burden and has inherently poor spatial resolution compared to CMR.

Echocardiography can be used to evaluate LV function with high temporal resolution and essentially no biological risk. However, the application of echocardiography may be impaired by the depth of tissue penetration of the ultrasound beam and the limited availability of adequate acoustic windows. Echocardiography is highly operator dependent, requiring manipulation of the ultrasound transducer by a skillful sonographer. Also, echo measurements of RV and LV volumes rely on geometrical assumptions based on a limited number of views, while CMR measures each ventricle in its entirety, slice-by-slice.

Although the absolute size of heart structures can be determined by CMR with high accuracy and reproducibility, it is well-established that the absolute sizes, volumes, and rates of cardiac parameters are strongly associated with body size.[33] Thus, a method to assess relative differences, independent of body size is desirable. The most common method to address this variability is by indexing to body surface area (BSA), though in some situations myocardial mass is referenced. Estimation of BSA itself is no trivial matter, often relying on approximations using formulas based on height/length, weight, or both. Allometric indexing of intracardiac areas to BSA during normal growth has also been validated, although linear dimensions should be indexed by the square root of BSA and volumes should be indexed by BSA to the 1.5 power.[34] Despite this limitation, normalization to BSA has proved useful for various measurements of the LV, RV, aortic root, and pulmonary vein.[34,35] Thus, normalization to BSA is the preferred approach when comparing cardiac structure and function parameters between sexes and during natural growth periods.

CMR is particularly useful for evaluating RV function. RV functional parameters are similar to those measured in the LV, including RV systolic and diastolic volumes, RV ejection fraction and stroke volume, and RV cardiac output. The combination of soft-tissue contrast and spatial resolution available with CMR makes it a useful tool for studying the changes in RV structure and function, mitigating the fact that the RV has a more complex geometry than the LV and a myocardial wall thickness that is often one-fifth that of the LV wall.[36] CMR has been used to measure RV functions in mice effectively.[37] CMR can produce reliable measurements of RV myocardial mass, which can inform our understanding of perinatal programming on cardiac development.[38] MRI-derived assessments of RV pressure–volume

loops can be constructed and used to evaluate RV contractility.[39] The CMR-derived ventricular mass index affords an accurate and practical method to noninvasively assess pulmonary artery (PA) pressure and may produce a more accurate estimate than Doppler echocardiography in pulmonary hypertension.[40]

CMR studies of the atria have mostly been applied to the left atrium (LA). The LA acts as a volume sensor, which through atrial stretching inhibits the secretion of vasopressin thus altering the RAS. Vasopressin's effects are mediated through several physiological mechanisms including escalation of arterial blood pressure, central blood volume, central venous pressure, and altering the sympathetic baroreflex set point.[41] Concurrently, left atrial stretching triggers the release of natriuretic peptides that decrease systemic vascular resistance, reduce central venous pressure, and increase the excretion of sodium by the kidneys.[42] Thus, it is not surprising that changes in LA size can be a biomarker for sustained elevations of LV filling pressures, especially in patients with heart failure with preserved ejection fraction complicated by hypertension.[43] Measures obtained by CMR include maximum/minimum LA volumes, total LA emptying volume and fraction, passive LA emptying volume and fraction, active LA emptying volume and fraction, and conduit volume. Changes in LA volume, indexed to myocardial mass, have been shown to be generally related to diastolic function in the normal population, although it may be predictive for more specific issues depending on the population being studied.[44] Right atrial (RA) volumes also have been investigated with CMR with regards to chronic heart failure and pulmonary hypertension. The utility of atrial imaging measurements in the setting of cardiac physiology altered by developmental programming in animal models has not yet been studied and is an emerging area of investigation.

Myocardial remodeling is a characteristic of developmental programming, which has been identified using echocardiography in fetuses and infants.[17] The "sphericity index" is used in echocardiography as an indicator of ventricular remodeling. Typically, in echocardiography studies, a sphericity index is approximated by calculation. Since CMR is used to measure the full ventricular volumes, the 3D sphericity index can be used, which is the ratio of the ventricular volume to the volume of a sphere that has the ventricular length as its radius.

In addition, CMR can be used to assess myocardial deformation. Myofibers in the mid-wall layer encircle the heart while longitudinal fibers in the endocardial and epicardial layers pull the heart from apex to base. The complex motion during contraction includes forces acting along a right-handed helix in the sub-endocardium but in a left-handed helix in the sub-epicardium. The resulting deformation, or "strains" can be resolved into components along with three directions: axial, circumferential, and longitudinal. Strain is defined in relation to the original length as a dimensionless percentage. The rate of deformation, "strain rate", is the spatial derivative of velocity and has units of inverse seconds. The initial method used a so-called "tissue tagging" approach, in which a special sequence "spoils" the magnetic nuclei so that lines of a null signal are deposited and tracked throughout the heart cycle.[45,46] A recent innovation, CMR feature tracking, evaluates anatomic elements that are different along the margins of the myocardium along the chamber wall/endocardium and epicardial/subepicardial boundaries. RV and LV systolic and diastolic function can be characterized using strain and strain rate as well as myocardial torsion and diastolic recoil. Myocardial

strain parameters from CMR studies produce more sensitive and earlier markers of contractile dysfunction than ejection fraction.[47] Fig. 2 displays examples of data obtained from myocardial feature tracking of LV cine images. Parameters measured include ventricular radial (Fig. 2a, c, e), circumferential, and longitudinal strains (Fig. 2b, d, f), strain rates, velocities, and displacements. Several commercially available image processing packages are available with feature tracking functionality.[48] Speckle tracking echocardiography has also been used to assess myocardial strain. However, the echo speckle results do not directly correspond to the MRI results. This may be due to the inherent sensitivity of echo speckle to noise and/or the relatively poor lateral resolution of the method.[49]

CMR also can be used to assess the focal or diffuse expansion of the myocardial extracellular space, which may result from prior infarction, infection, or other causes of tissue composition derangement. Hematocrit (hct) should be gathered on the same day as the MRI examination as it can fluctuate. Following administration of intravascular gadolinium contrast agent and a time delay (>10 min), focal scarring/extracellular space expansion can be directly visualized and quantified. For evaluation of diffuse extracellular space expansion, the longitudinal relaxation time ($T1$) of the myocardium and the $T1$ of blood in the ventricular lumen must be measured (Fig. 3a, b). In a common protocol, myocardial $T1$ is measured again ~10 min after administration of a gadolinium contrast agent.[50] From these datasets, and the patient's hct, the extracellular volume (ECV) of the myocardial tissue can be calculated as: myocardial $ECV = (1-hct) \times \Delta\ T1_{blood})/(\Delta\ T1_{myocardium})$. ECV was found to be directly associated with myocardial fibrosis related to aging in a large human study.[51] Diffuse myocardial fibrosis is believed to be one of the conditions associated with impaired ventricular function due to developmental programming. An example of how myocardial $T1$ is altered ~10 min after Gd infusion in the baboon heart is shown in Fig. 3. A more advanced approach, diffusion tensor CMR (DT-CMR), can be used to evaluate myocyte orientation and sheetlet function, however this a technically challenging method.[52] New approaches that combine improved spatial and angular resolution with greater scanning speed and increased coverage may allow DT-CMR to become a routine research tool in the near future. The power of sampling myocardial tissue at necropsy in animal models of developmental programming can be used to correlate features such as fibrosis with *in vivo* images of the tissue structure.[14]

MRI is also useful for differentiating between muscle tissue and fat, making it useful for discerning fatty infiltration of the myocardium. Epicardial fat and pericardial adiposity, which are common in patients with insulin resistance, have been associated with a number of cardiovascular conditions.[53] Increased pericardial fat deposition, measured by CMR has been reported in male IUGR baboons, but not females at 5–6 years (human equivalent 20–24 years).[54] Volume-localized magnetic resonance spectroscopy (MRS) can be used to determine the amount of fat within the myocardium (Fig. 4a), although the process is more time-consuming and technologically demanding.[55] Fig. 4 depicts an example of a hydrogen-1 CMR spectrum obtained from the interventricular septum of a baboon heart. Note that there are three triglyceride peaks (Fig. 4b). However, due to the complex myofiber orientations in heart muscle, MRS measures total fat and cannot yet distinguish intra- and extracellular lipids, which may have different metabolic origins.[56]

CMR can also be used to measure blood flow, although not with the same temporal resolution afforded by Doppler echocardiography. Phase-contrast MRI can be used to measure the velocity of flowing blood in the great vessels or smaller arteries by relating the change in phase of the MRI signal from blood to the change in position of the blood. Because imaging slices can be positioned flexibly and accurately, CMR can provide precise measures of cardiac output and coronary blood flow.[57,58] CMR is used to determine aortic compliance and flow across the mitral valve. Aortic distensibility can be calculated from measurements of the cross-sectional area of the distal descending aorta at the level of the heart, taken at ES and ED.[57] Distensibility is defined as the fractional decrease in aortic area divided by the difference between systolic and diastolic blood pressure. Pharmaceutical agents, such as dobutamine and adenosine, can be infused during CMR to assess myocardial perfusion during vasodilation and myocardial function during cardiac stress.[59] 4D flow MRI combines three-dimensional spatial encoding combined with three-directional velocity-encoded phase-contrast MRI allowing quantitative visualization of complex, three-directional blood flow patterns in vascular structures and entire vascular territories such as the heart, the adjacent aorta, and coronary arteries.[60] These approaches allow assessments of cardiac performance under physiological conditions that normally occur with increasing workloads.

The Society for Cardiovascular Magnetic Resonance (SCMR) has developed an expert consensus report that assesses evidence of the accuracy and precision of CMR-derived cardiovascular parameters.[61] Although these parameters were considered in the context of diagnosing and evaluating disease severity, the report clarifies the strengths and weaknesses of modern, quantitative CMR. Data presented in the SCMR report have been compiled and summarized in Table 1.

Normative values of CMR parameters

As delineated above, quantitative CMR can provide a multitude of data, not only with regard to chamber sizes and function, but also concerning the regional function of the heart, blood flow, and tissue composition. A recent review of published data lists reference values and influencing factors, such as age and sex, on normative cardiac physiological parameters derived from various CMR techniques and pulse sequences.[62]

A recent study of 800 adult UK subjects evaluated CMR data from healthy Caucasian British participants in order to establish reference values and abnormal ranges, for LV, RV, LA, and RA structure and function.[63] Bland–Altmann analyses of these data found that for LV and RV end-diastolic volume, end-systolic volume, and stroke volume and LA and RA maximal volume and stroke volume, excellent inter- and intra-observer agreement was achieved. Another study reported the same cardiovascular parameters from CMR, but focused on over 400 healthy Caucasian participants between the ages of 18 and 36 years.[64] Using both intra-class correlation coefficients (ICC) and by the Bland–Altman method, these investigators showed that LV and RV EDV has biases ≤2.3ml, LA and RA EDV have biases <6.5 ml, and all had ICC values ≥0.92. Two other investigations have aimed to establish normative ranges for RA and LA structural and functional parameters normalized for independent influences such as age, sex, and BSA. One studied 120 asymptomatic medical

workers in Great Britain[65] and the other assessed 115 healthy children and adolescents in Germany.[66,67] The latter study found high interobserver and inter-examination agreement by the Bland–Altman method, even for pediatric subjects. BSA-indexed normative cardiac functional data by age group reported from these studies have been compiled in Tables 2–4.

The studies, cited above, primarily report data from North American and European Caucasian cohorts. A direct comparison between four American ethnicities (Caucasian, Hispanic, African-American, and Asian-American) showed that Asian-American participants, in general, had lower values for LV mass and volumes than other ethnic groups even when adjusted for BSA.[68] A more recent study from the same group found that LA volume also was smaller in Chinese-American subjects even after allometric indexing.[69] A comprehensive study of 20–69-year-old Singaporean Chinese subjects ($n = 180$) found smaller cardiac volumes (LV EDV: 128 ± 28 vs. 146 ml; RV EDV: 143 ± 35 vs. 162 ml) and lower LV mass (76 ± 22 vs. 116 g). These differences remained after normalizing for BSA but, as in Caucasians, negative correlations between ventricular volumes and age were found without associations between LV mass and age.[70] Further studies are required to understand the normative age-related variability of normal cardiac structure and function across diverse ethnic groups.

MRI tissue parameters also have been measured by CMR. The MRI relaxation times, $T1$, $T2$, and $T2^*$, can be determined in myocardium using specialized pulse sequences that measure the changes in the CMR signal with changes in acquisition timing parameters.[71] Relaxation measurements require multiple rescans using different timing parameters in order to derive the relaxation times from the signal intensity versus time curves via nonlinear regression as shown in Fig. 3c. $T1$ increases with the magnetic field strength used for MRI, but also is associated biologically with disease states that lead to fibrosis, edema, and amyloid deposition. $T1$ is reduced by administration of a gadolinium-based contrast agent (Gd), which briefly is retained in the interstitial space.[72] By making measurements before and after Gd, the ECV can be determined and used as a biomarker for myocardial fibrosis (Fig. 3). A study conducted at 3 Tesla in a cohort ($n = 76$) of asymptomatic volunteers 20–90 years of age-reported native myocardial $T1$ and ECV, but not $T2$, were significantly greater in age-matched women than in men.[73] In addition, $T1$ and ECV increased with increasing age. However, in children (aged 9–18) $T1$ did not change with age but was significantly correlated ($r = 0.448$, $p - 0.005$) with body mass index (BMI).[74] Although apposite interobserver variability has been reported for myocardial $T1$ measurements with ICC > 0.90,[75] for multicenter investigations, it is good practice to certify that the $T1$ mapping method utilizes a standardized acquisition and post-processing approach.[76]

Studies also have evaluated $T2$, which increases with water content in myocardial tissues, as in myocardial edema. $T2$ is reported to decrease significantly with increasing age.[73] Decreases in the related parameter, myocardial $T2^*$, have been associated with iron deposition which is indicative of thalassemia in children.[77] A high-field (7 T) study of chicken embryos reported that $T2$ in the heart and other organs decreased during embryonic development.[78] In a Polish study of 41 healthy children, 9–18 years old, myocardial $T2$ was found to be significantly higher (44.6 ± 4.2 vs. 40.4 ± 3.8 $p = 0.002$) in females than in males.[74] Normative values of $T1$, $T2$, and $T2^*$ for various age groups are listed in Table 5.

The development of the heart in early childhood has also been studied using CMR. Most of these studies have focused on infants with congenital heart diseases such as patent ductus arteriosus (PDA) and preterm infants. In studies of extremely young subjects, cardiac dimension measurements are typically indexed to body weight. Indexed cardiac parameters were significantly greater in a group of 16 PDA infants compared to 29 control infants in a study that showed good intra- and interobserver agreement.[79] These parameters included LV stroke volume (2.81 ± 0.83 vs. 1.82 ± 0.29 ml/kg, $p < 0.001$), end-diastolic volume (3.38 ± 1.34 vs. 2.47 ± 0.38 ml/kg, $p = 0.001$), and LV mass (2.46 ± 0.59 vs. 1.39 ± 0.23 g/kg, $p < 0.001$). However, there were no significant differences in ejection fraction or fractional thickening between the two groups. Currently, studies of RV function and structure in infants have not demonstrated adequate reproducibility.

CMR was used to measure cardiac output and tricuspid and mitral E/A trans-mitral waveforms with Doppler at median 30.4 weeks gestational age (95% range 28.4–32.7), and then again at a median age of 10.0 years (95% range 9.4–11.7) in 547 subjects.[80] These investigators found that higher third-trimester umbilical artery resistance was associated with higher childhood RV EF ($p < 0.05$), but not with other cardiac outcomes. The third-trimester umbilical artery to cerebral artery pulsatility index ratio was not associated with childhood cardiac outcomes. Higher third-trimester fetal LV output was associated with lower childhood LV EF and higher LV mass-to-volume ratios ($p < 0.05$). Third-trimester fetal RV output was not associated with childhood cardiac outcomes. A higher third-trimester fetal tricuspid valve E/A mitral waveform ratio was associated with higher childhood RV EF ($p < 0.05$).

Through-plane phase-contrast MRI velocity measurements have been used to assess left and right ventricular output in preterm and term newborns in a neonatal unit.[81] PA pulse wave velocities, measured in children (ages 9–12-year-old) using velocity-encoded MRI, have been shown to be reproducible and sufficiently sensitive to detect differences in PA compliance between normoxia and hypoxia.[82] CMR-derived longitudinal, radial, and circumferential strain measurements also have been characterized recently in children.[83]

CMR developmental programming phenotypes

Quantitative CMR in fetal hearts, including cardiac function, blood flow, and blood oxygenation, is an area of active development. The high resolution demanded in fetal hearts can be confounded by the need to avoid aliasing artifacts from other parts of the mother's body. However, the primary technical challenge is to deal with the various sources of motion artifacts which include cardiac and respiratory motion of the mother, cardiac motion of the fetus, and fetal body motion. Innovations such as metric-optimized gating, self-gating, and the development of MRI-compatible fetal heart monitoring hardware allow fetal CMR to be more tolerant to motion, thereby allowing high-resolution dynamic imaging of the fetal heart and its associated vessels.[84] With adequate control for physiological motion, fetal ventricular volumetry has been shown to be very reliable in the sheep model.[85] The development of 4D cine methods, using highly accelerated dynamic MRI with slice-to-volume reconstruction, can capture fetal cardiac motions in real-time.[86] The use of 4D flow CMR has been validated for directly measuring flow through fetal vessels of the central circulation and their

shunts in an *in utero* sheep model.[87] Also, *T*2 relaxometry measurements have been used in fetal sheep models to quantitate blood oxygenation with CMR and validate these against blood gas analyzer measurements.[88] These methods have been applied to assess cardiac function in a study of late-onset IUGR human fetuses with reported values indexed to estimated fetal weight. Reduced umbilical vein and pulmonary blood flow, along with increased superior vena caval flow, were found in IUGR compared to normal fetuses.[89] Also, blood *T*2 values, oxygen delivery, and oxygen consumption were significantly lower in the IUGR fetuses. The development of reliable CMR methods for assessing fetal hemodynamics and morphometrics will provide more reliable data for understanding the development of IUGR *in utero* and allow improved classification of IUGR at the early stages of pregnancy.

CMR has shown that small size for gestational age (SGA) at birth was associated with smaller LV and RV end-diastolic volume relative to current BSA, but with larger LV mass-to-volume ratio ($p < 0.05$). Children in the larger quartile at birth who grow taller and leaner in childhood have larger hearts relative to BSA. In contrast, children in the lower quartile of RV and LV end-diastolic volume and LV mass were smaller at birth and became shorter and heavier in childhood ($p < 0.05$). Both fetal and childhood growth were independently associated with childhood RV and LV end-diastolic volume and LV mass.[90]

In a CMR study of 29 fetuses with IUGR compared to 127 fetuses with various congenital heart diseases, IUGR fetuses were significantly heavier than fetuses with transposition of the great arteries ($p = 0.03$) and coarctation of the aorta ($p = 0.02$), but there were no significant fetal body weight differences between IUGR and other congenital heart diseases.[91] The same group studied 14 IUGR and 26 non-IUGR fetuses at 35 weeks' gestation using MRI, reporting that IUGR fetuses had lower umbilical vein ($p < 0.004$) and pulmonary blood flow ($p < 0.01$) and higher superior vena caval flow ($p < 0.0001$).[89] The latter change is exemplary of the classical preferential delivery of blood to pre-ductal vascular beds in the presence of intrauterine challenges.[92]

A recent study of 34 preterm infants and 10 term controls reported greater CMR weight-indexed LV mass and higher weight-indexed end-diastolic volume at term-corrected age ($p < 0.05$ for all preterm gestations).[93] Independent associations of increased term-corrected age LV myocardial wall thickness were (false discovery rate <0.05): degree of prematurity, antenatal glucocorticoid administration, and a requirement for >48 h postnatal respiratory support. Principal component analysis of LV volumes, geometry, myocardial mass, and wall thickness revealed statistical differences between all preterm infants at term-corrected age and term controls.[93]

Intrauterine growth restriction due to reduced maternal nutrition and cardiac health in baboon offspring

Investigations of the effects of developmental programming need to consider the species and sex of offspring differences in outcomes. The common experimental model of the laboratory rat is a polytocous, altricial species. Mothers, thus, nurture a much larger nutritional load and fetuses and neonates have a different trajectory of development from monotocous, precocial

mammals such as humans.[94] For this reason, a nonhuman primate, baboon model has been developed and characterized.[95] Molecular techniques were used to evaluate the functional, biochemical, and epigenetic mechanisms and interactions in the heart that result from the challenge of maternal undernutrition and obesity from overnutrition.[14,15]

CMR has been extensively applied in this IUGR baboon model to study CV changes that arise from developmental programming secondary to moderate (30%) MNR during pregnancy and lactation. Both LV and RV function were impaired in the offspring, including decreased ejection fractions, ventricular shortening, and increased chamber volumes.[38,96] Fig. 5 illustrates differences in the BSA-normalized LV volume–time curves obtained by CMR over the cardiac cycle control and IUGR baboons, differentiated by sex. The results underscored that MNR affected RV function more drastically than the LV function. The severity of the impairment in RV function may be due to increased pulmonary resistance, which would be attributed to decreased fetal pulmonary alveolarization, and pulmonary vessel density, found in a sheep model of IUGR.[97] While these data have been interpreted as indicating that growth restriction mimics accelerated aging of the heart, the most essential finding was the interplay and synergistic effect of these changes toward jeopardizing overall cardiovascular health.

Changes in heart morphology and function that are expected to be associated with broader cardiovascular features also can be assessed using CMR. Distal descending indexed aortic cross section and aortic distensibility were decreased in the same IUGR baboons.[98] Fig. 6 depicts how the increased systolic 3D sphericity index (3DSI) was significantly correlated with reduced aortic distensibility ($r = 0.35$, $p = 0.048$). Diastolic 3DSI also was significantly and negatively correlated with aortic distensibility ($r = 0.36$, $p = 0.044$). Complementary changes in carotid, brachial, and iliac artery sizes, distensibility, and blood flow pattern also have been identified in young adult IUGR baboons using ultrasound.[99]

The biventricular changes signify the core components of the observed findings. In the LV, there is impairment of myocardial contraction. Based on studies from other animal models of poor maternal nutrition, the weakened contraction may be due to diminished cardiomyocyte number,[100,101] cardiomyocyte immaturity, [102,103] abnormal calcium handling,[104] and/or sarcomere dysfunction. [105] With this decrease in contractile force, an increase in end-systolic volume is seen with MRI without significant modification in the end-diastolic volume, resulting in decreases in stroke volume and cardiac output. The decreased wall thickening fraction and trend of reduced rotation together suggest a decline in systolic function. Due to the increased end-systolic volume, there is increased difficulty in LV filling, reflected by a prominent decrease in peak and average filling function.

The struggle to fill the LV may be further compromised by extracellular fibrosis previously seen in the fetal baboon myocardium and as reported in other models.[14,106] A study on 36 patients with dilated cardiomyopathy (DCM) examined the degree to which native myocardial $T1$ could be used to characterize collagen volume fraction measurement from histology.[107] These investigators found that the native myocardial $T1$ value was significantly and positively correlated with biopsy-proven collagen volume fraction ($r = 0.77$, $p < 0.01$).

We have measured native myocardial *T*1 to be significantly greater in IUGR baboons (1033 + 93ms) than in controls (905 +93 ms, $p = 0.001$), Fig. 7.

The LV systolic and diastolic function abnormalities as a result of IUGR may originate from cardiomyocyte changes discussed in prior reports. The relationship between RV and LV dysfunction is depicted schematically in Fig. 8. The contractile force of the RV was weakened as in the left, supported by decreases in both wall thickening and longitudinal shortening seen on MRI. RV end-systolic volume increased, and RV stroke volume and cardiac output fell. An attempt to increase the ejection function in the form of a mild increase in end-diastolic volume is suspected. Nonetheless, the increased end-systolic volume from inadequate ejection hinders RV filling, reducing both average and early filling rates. Although decreased sphericity indices are anticipated based on LV sphericity increase, no such difference is seen. This finding likely represents simultaneous RV congestion. Importantly, the impaired LV filling may further deteriorate RV ejection via increasing pulmonary pressure.[108] These findings are consistent with impairment of coronary filling and mild hypoxia can be suspected, given the probable rise in diastolic pressure.

On the mechanical level, weakening of one ventricular chamber's contraction aggravates the other, as normally the cardiac longitudinal shortening force depends on concurrent pull of both the mitral and tricuspid annuli. Exaggerated septal movement toward the LV during systole, which normally only accounts for ~10% RV stroke volume, is interpreted as an attempt to normalize LV ejection, which may hamper RV ejection. Decreased LV systolic function also results in a weakening of the RV output due to ventricular interdependence. The more pronounced decrease in RV function, compared to the LV, indicates a primary component of RV dysfunction is present, which may originate in part from changes in the pulmonary system. However, the status of the RV myocardium and its relationship to pulmonary arterial dysfunction remain to be investigated given the lack of sufficient prior studies.

In the IUGR baboon model, the large systemic arteries demonstrated regional divergent findings. MRI revealed the descending thoracic aorta was decreased in size and distensibility. These decreases diminished the aortic Windkessel function and raised concern for diastolic perfusion of critical organs.[98] In particular, coronary perfusion is likely to be compromised given its predominantly diastolic filling pattern. Additionally, the decreased size and distensibility of the descending aorta, combined with similar changes in the lower extremity arteries uncovered by ultrasound, indicated systemic afterload was likely elevated, contributing to LV dysfunction. Various animal studies have implicated decreased elastin content[109] as well as changes in extracellular structure[110,111] in contributing to the observed changes. In the cranially directed vessels, however, neither difference in size nor distensibility is seen. Instead, the overall carotid blood flow appears preserved, or even increased, due to a mild increase in end-systolic and diastolic flowrates. This constellation of findings is reminiscent of the blood flow redistribution effort known to occur during fetal hypoxia as part of the "brain sparing" effect.[92] Following this analogy, the modification in blood flow in perinatal life would have triggered differential growth of the vasculature via hemodynamic effects, which persist into adulthood. There also may be involvement of

additional abdominal and pelvic vessels, which would have implications in other organ systems.

In the baboon model of IUGR, female offspring had increased total cholesterol, low-density lipoprotein, and subcutaneous fat. These changes were absent in male offspring, although MRI in the males did reveal increased pericardial fat depositions.[54] Metabolic derangements present in IUGR are detected in the form of a sexually dimorphic increase in pericardial lipid accumulation and serum cholesterol level. These increases were mild, especially when compared to the extent of cardiac changes observed. However, the increased pericardial lipids, if left untreated, may result in local lipotoxic effects later in the life course. The increase in serum cholesterol can contribute to the development of coronary atherosclerosis.

Future applications of CMR in the study of cardiac programming

The flexibility of cardiac MRI allows it to interpret the complex interactions of biomarkers related to IUGR pathophysiology, for example, the interplay between IUGR and accelerated aging. Prenatal programming is associated with the development of myocardial fibrosis, which is attributed, in large part, to epigenetic processes.[14,15] Physiological trajectories are altered as an adaptive response to maintain the fetus for a successful birth. However, there is strong evidence that these early life adaptations reduce the individual's flexibility to respond to age-associated changes in cardiovascular structure and function in later life. Adverse remodeling is rooted in dysfunctional repair mechanisms that protect the heart from further injury and enhance homeostasis.[112]

In the baboon IUGR model, we have defined an extensive cardiac functional phenotype at baseline under sedation. Unfortunately, we have yet to study cardiac function under various other challenges. In humans, the resting cardiac functional measurements do not always correlate with those obtained under stress. For instance, aging weakens LV ejection under stress but not at rest, whereas exercise training lowers resting ejection function without affecting stress values. Cardiac MRI evaluations could be performed during pharmacological stress using, for example, dopamine which should help better define the physiologic impact of the observed findings. Biomarkers, such as peak circumferential strain, average diastolic strain rate, contractile reserve, and myocardial blood flow were reported to be robust with good interobserver and intra-observer reproducibility and test-retest reliability during pharmacologically induced stress in healthy male (7–10 years old) macaques.[113]

Currently, it is unclear what tissue changes contribute to the ventricular dysfunction. Whether the LV extracellular space expansion, previously seen in the fetal heart, persists into adulthood or occurs in the RV has not yet been determined. In addition to measuring the myocardial $T1$ relaxation time by MRI, cardiac diffusion tensor imaging (DTI) can be used to examine the myocyte architecture and fiber orientation to identify the presence of pathology and/or extracellular space expansion more precisely. Cardiac DTI can also improve our understanding of the mechanisms and structural contributions related to atrial rhythm and pump disorders.[114] Although technically challenging due to heart and respiratory motion, new accelerated DTI pulse sequences and advanced image reconstruction technologies improve the accuracy and efficiency of diffusion CMR.[115]

The finding of reduced RV ejection fractions and systemic vascular alteration in offspring of MNR mothers indicates pathophysiology in the pulmonary system that merits investigation particularly in relation to the rapid changes in pulmonary blood flow that take place at birth. In fetal sheep, an increase in myocardial fibrosis has been reported in the RV after maternal undernutrition.[116] Dynamic perfusion MRI can quantitatively analyze regional pulmonary perfusion[117] and may be helpful in this endeavor. Likewise, the finding of impaired aortic Windkessel function suggests studies such as MRI evaluation of the coronary arterial perfusion[118] and oxygenation[119] also could be beneficial, given the extensive literature on ischemic heart disease risk with IUGR.

MRI also can be used to evaluate related noncardiac conditions that are closely associated with developmental programming. An early and persistent finding has been the increased prevalence of idiopathic hypertension in people with low birth weight. This observation has led to studies in human and animal models that were aimed at discerning the relationships between CVD and kidney disease. IUGR has been linked with a reduction in renal cell size and number that, in turn, has been implicated in renal dysfunction and the occurrence of systemic hypertension. In the baboon IUGR model, it was found that midgestational IUGR fetal kidneys showed down-regulation of genes in pathways related to RNA, DNA, and protein biosynthesis. In addition, upregulation in cell signal transduction, communication, and transport were reported.[120] Thus, even a challenge of moderate maternal global nutrient restriction causes significant changes in fetal renal gene pathways. Renal perfusion can be evaluated quantitatively using various MRI methods, including dynamic contrast-enhanced MRI, arterial spin labeling, and diffusion-weighted MRI.[121] Moreover, blood oxygen level-dependent (BOLD) MRI, which exploits deoxygenated hemoglobin's paramagnetic influence on the MRI signal, can be used to gain insights on tissue oxygenation.[122,123]

Epidemiological evidence also implicates low birth weight as a risk factor for the development of diabetes. The relationship between CVD and metabolic disease is well-established and has been labeled the metabolic syndrome. Three of the five hallmarks of the metabolic syndrome are related to lipid function: central obesity, high serum triglycerides, and low serum high-density lipoprotein. Maternal obesity during pregnancy has been linked to increase offspring insulin resistance in humans.[124] In the IUGR baboon model, MNR in pregnancy and lactation were found to program offspring metabolic responses, including insulin resistance and β-cell responsiveness that lay the foundation of an overall phenotype that can predispose to later life type-2 diabetes.[125] MRS methods for assessing cardiomyocyte lipids[126] and phosphorus energetics[127] have been developed and could be used to help understand the synergistic effects of fetal programming on cardiovascular function and metabolism.

However, the full range of CMR capabilities, which could reveal new information on the IUGR cardiovasculature has not yet been applied at a large scale. Quantitative procedures to assess heart physiology, which are available and clinically validated, have not yet been exploited to better understand the processes underlying normal and divergent development. Current studies have been limited to technologies that have explored only the most basic physiology related to cardiovascular developmental programming.

In conclusion, cardiac MRI encompasses methods that are largely noninvasive and easily translatable from rodents to nonhuman primate models to human studies. Investigations into humans, which parallel those in animal models, are now possible and given the compelling evidence that prenatal challenges lead to later life CVD and have features of premature cardiac aging, the information obtained will accelerate our understanding of the mechanism of developmental programming and programming– aging interactions in the onset of later life CVD. The MRI biomarkers identified from animal models can be combined with tissue and cellular biomarker information to allow earlier identification of individuals at risk and enable assessment of treatment needs and therapeutic response. Ideally, the knowledge gained will lead to better clinical management of this vulnerable population. The strengths of investigating animal models include having homogeneity of subjects and greater control over environmental and genetic confounds. Animal studies also give us the ability to undertake a greater degree of invasiveness and more frequent repetition across the life course and greater flexibility for therapeutic trials.

However, to fully utilize the potential of MRI, the application of standardized protocols must be applied to larger human populations in order to characterize the true nature of CV health and disease. In some areas of biomedicine, particularly in neuroscience, the widespread use of MRI to define normal and abnormal human phenotypes have been undertaken. The Human Connectome Project (https://www.humanconnectome.org), established by the National Institutes of Health in the US, is a multinational and multi-institutional program that utilizes advanced MRI technologies to study over 1200 subjects, focusing on various processes and pathologies involving the human brain, especially those associated a with aging. Other national and international projects of similar scope include the German 1000BRAINS study and the UK Biobank. Recently, the Lifespan Human Connectome Project in Development, a large-scale study of brain connectivity in over 1300 subjects of ages 5–21 years, has been established[128] and the Lifespan Developing Human Connectome Project at Kings College, UK will perform MRI of human brain connectivity in 1500 subjects with post-conceptional ages ranging from 20 to 44 weeks. (https://www.humanconnectome.org/study/lifespandeveloping-human-connectome-project).

The prospect of using MRI to improve understanding of brain changes with early development is important since changes in brain macrostructure, microstructure, and hemodynamics have all been documented in human fetuses and infants with late-onset IUGR.[89,129,130]

However, there is not yet any organized effort to evaluate fetal heart development with CMR. Although CMR has become an important component of the Framingham Heart Study in the US[131] and the Dutch Heart-Brain Study,[132] these megaprojects have focused mostly on adults with various pathologies, without consideration of their early developmental histories. In order to fully appreciate the settings and consequences of developmental programming on CVD in the real world, a larger multinational human study that uses cardiac MRI to investigate CV development, including prenatally, should be undertaken. The results of such an effort, in combination with advanced omics testing, would advance the quest for a clear, clinical definition of IUGR. In addition, the data obtained would produce a

wealth of information that would not only inform allopathic medicine, but also preventative medicine and public health worldwide.

Acknowledgments.

We thank the research team at the Texas Center for Reproductive Health, which includes Dr. Cun Li, Dr. Hillary Huber as well as the administrative support of Karen Moore. The authors also thank Dr. Deepak Kaushal and the Southwest National Primate Center Staff for their ongoing support of the baboon research program described in this article. The authors also acknowledge the animal technical and veterinary support of the Texas Biomedical Research Institute staff.

Financial support. This research program described in this work was supported by the Julio C. Palmaz Endowment for Excellence in Radiology Research Pilot Grant-AHK. Furthermore, this work was supported by the National Institutes of Health 5P01HD021350 – PWN, 1U19AG057758-01A1, 5R24OD011183 – PWN, OD P51 OD011133 – GDC, 1R25EB016631 – AHK, and EU FP 7/HEALTH/GA No. 279,281: BrainAge – Impact of Prenatal Stress on BRAINAGEing.

References

1. Barker DJ. Fetal nutrition and cardiovascular disease in later life. Brit Med Bul. 1997; 53, 96–108.
2. Dong M, Zheng Q, Ford SP, Nathanielsz PW, Ren J. Maternal obesity, lipotoxicity and cardiovascular diseases in offspring. J Mol Cell Cardiol. 2013; 55, 111–116. [PubMed: 22982026]
3. Roseboom TJ, van der Meulen JH, Osmond C, et al. Coronary heart disease after prenatal exposure to the Dutch famine, 1944–45. Heart. 2000; 84, 595–598. [PubMed: 11083734]
4. Barker DJ, Bagby SP. Developmental antecedents of cardiovascular disease: a historical perspective. J Am Soc Nephrol. 2005; 16, 2537–2544. [PubMed: 16049070]
5. Gluckman PD, Hanson MA, Buklijas T, Low FM, Beedle AS. Epigenetic mechanisms that underpin metabolic and cardiovascular diseases. Nat Rev Endocrinol. 2009; 5, 401–408. [PubMed: 19488075]
6. Agarwal P, Morriseau TS, Kereliuk SM, Doucette CA, Wicklow BA, Dolinsky VW. Maternal obesity, diabetes during pregnancy and epigenetic mechanisms that influence the developmental origins of cardiometabolic disease in the offspring. Crit Rev Clin Lab Sci. 2018; 55, 71–101. [PubMed: 29308692]
7. Nathanielsz PW. Life in the Womb: The Origin of Health and Disease, 1999. Promethean Press, Ithaca, NY.
8. Watson CJ, Collier P, Tea I, et al. Hypoxia-induced epigenetic modifications are associated with cardiac tissue fibrosis and the development of a myofibroblast-like phenotype. Hum Mol Gen. 2014; 23, 2176–2188. [PubMed: 24301681]
9. Lee L, Lupo P. Maternal smoking during pregnancy and the risk of congenital heart defects in offspring: a systematic review and metaanalysis. Pediatr Cardiol. 2013; 34, 398–407. [PubMed: 22886364]
10. Reid N, Akison LK, Hoy W, Moritz KM. Adverse health outcomes associated with fetal alcohol exposure: a systematic review focused on cardio–renal outcomes. J Stud Alcohol Drugs. 2019; 80, 515–523. [PubMed: 31603752]
11. Govindsamy A, Naidoo S, Cerf ME. Cardiac development and transcription factors: insulin signalling, insulin resistance, and intrauterine nutritional programming of cardiovascular disease. J Nutr Metab. 2018; Article ID 8547976, 12.
12. Blackmore HL, Ozanne SE. Programming of cardiovascular disease across the life-course. J Molec Cell Cardiol. 2015; 83, 122–130. [PubMed: 25510678]
13. van der Harst P, de Windt LJ, Chambers JC. Translational perspective on epigenetics in cardiovascular disease. JACC. 2017; 70, 590–606. [PubMed: 28750703]
14. Muralimanoharan S, Li C, Nakayasu ES, et al. Sexual dimorphism in the fetal cardiac response to maternal nutrient restriction. J Mol Cell Cardiol. 2017; 108, 181–193. [PubMed: 28641979]

15. Maloyan A, Muralimanoharan S, Huffman S, Cox LA, Nathanielsz PW, Myatt L, Nijland MJ. Identification and comparative analyses of myocardial miRNAs involved in the fetal response to maternal obesity. Physiol Genomics. 2013; 45: 889–900. [PubMed: 23922128]
16. Alfonso F, Macaya C, Goicolea J, In A, Hernandez R, Zamorano J, Perez-Vizcayne MJ, Zarco P. Intravascular ultrasound imaging of angiographically normal coronary segments in patients with coronary artery disease. Am Heart J. 1994; 127, 536–544. [PubMed: 8122599]
17. Crispi F, Miranda J, Gratacos E. Long-term cardiovascular consequences of fetal growth restriction: biology, clinical implications, and opportunities for prevention of adult disease. Am J Obstet Gynecol. 2018; 218, S869–S879. [PubMed: 29422215]
18. Rodríguez-López M, Cruz-Lemini M, Valenzuela-Alcaraz B, et al. Descriptive analysis of different phenotypes of cardiac remodeling in fetal growth restriction. Ultrasound Obst Gyn. 2017; 50, 207–214.
19. Comas M, Crispi F, Cruz-Martinez R, Figueras F, Gratacos E. Tissue Doppler echocardiographic markers of cardiac dysfunction in small-for-gestational age fetuses. Am J Obstet Gynecol. 2011; 205, 57–e1. [PubMed: 21620362]
20. Cruz-Lemini M, Crispi F, Valenzuela-Alcaraz B, et al. Fetal cardiovascular remodeling persists at 6 months in infants with intrauterine growth restriction. Ultrasound Obst Gyn. 2016; 48, 349–356.
21. Sehgal A, Doctor T, Menahem S. Cardiac function and arterial biophysical properties in small for gestational age infants: postnatal manifestations of fetal programming. J Pediatr. 2013; 163, 1296–1300. [PubMed: 23896189]
22. Rueda-Clausen CF, Morton JS, Dolinsky VW, Dyck JR, Davidge ST. Synergistic effects of prenatal hypoxia and postnatal high-fat diet in the development of cardiovascular pathology in young rats. Am J Physiol Regul Integr Comp Physiol. 2012; 303, R418–R426. [PubMed: 22739349]
23. Aljunaidy MM, Morton JS, Kirschenman R, et al. Maternal treatment with a placental-targeted antioxidant (MitoQ) impacts offspring cardiovascular function in a rat model of prenatal hypoxia. Pharm Res. 2018; 134, 332–342.
24. Zohdi V, Pearson JT, Kett MM, et al. When early life growth restriction in rats is followed by attenuated postnatal growth: effects on cardiac function in adulthood. Eur J Nutr. 2015; 54, 743–750. [PubMed: 25115176]
25. Keller AM, Peshock RM, Malloy CR, et al. In vivo measurement of myocardial mass using nuclear magnetic resonance imaging. J Am Coll Cardiol. 1986; 8, 113–117. [PubMed: 3711507]
26. Buser PT, Auffermann W, Holt WW, Wagner S, Kircher B, Wolfe C, Higgins CB. Noninvasive evaluation of global left ventricular function with use of cine nuclear magnetic resonance. JACC. 1989; 13, 1294–300. [PubMed: 2703612]
27. Soldo SJ, Norris SL, Gober JR, et al. MRI-derived ventricular volume curves for the assessment of left ventricular function. Magn Reson Imag. 1994; 12, 711–717.
28. Spielmann RP, Schneider O, Thiele F, Heller M, Bücheler E. Appearance of poststenotic jets in MRI: dependence on flow velocity and on imaging parameters. Magn Reson Imag. 1991; 9, 67–72.
29. Peng P, Lekadir K, Gooya A, Shao Ling, Petersen Steffen E, Frangi Alejandro F. A review of heart chamber segmentation for structural and functional analysis using cardiac magnetic resonance imaging. Magn Reson Mater Phy. 2016; 29, 155–195.
30. Heiberg E, Sjögren J, Ugander M, Carlsson M, Engblom H, Arheden H. Design and validation of segment: freely available software for cardiovascular image analysis. BMC Med Imag. 2010; 10, 1–13.
31. Leng S, Ge H, He J, et al. Long-term prognostic value of cardiac MRI left atrial strain in ST-segment elevation myocardial infarction. Radiology. 2020; 296, 299–309. [PubMed: 32544032]
32. Trattner S, Chelliah A, Prinsen P, et al. Estimating effective dose of radiation from pediatric cardiac CT angiography using a 64-MDCT scanner: new conversion factors relating dose-length product to effective dose. AJR Am J Roentgenol. 2017; 208, 585–594. [PubMed: 28095022]
33. Kleiber M Body size and metabolic rate. Physiol Rev. 1947; 27, 511–541. [PubMed: 20267758]
34. Gutgesell HP, Rembold CM. Growth of the human heart relative to body surface area. Am J Cardiol. 1990; 65, 662–668. [PubMed: 2309636]

35. D'Oronzio U, Senn O, Biaggi P, et al. Right heart assessment by echocardiography: gender and body size matters. J Am Soc Echocardiog. 2012; 25, 1251–1258.
36. Beygui F, Furber A, Delépine S, et al. Routine breath-hold gradient echo MRI-derived right ventricular mass, volumes and function: accuracy, reproducibility and coherence study. Int J Cardiovasc Imag. 2004; 20, 509–516.
37. Wiesmann F, Frydrychowicz A, Rautenberg J, et al. Analysis of right ventricular function in healthy mice and a murine model of heart failure by in vivo MRI. Am J Physiol Heart Circ Physiol. 2002; 283, H1065–H1071. [PubMed: 12181136]
38. Kuo AH, Li C, Huber HF, et al. Maternal nutrient restriction during pregnancy and lactation leads to impaired right ventricular function in young adult baboons. J Physiol. 2017; 595, 4245–4260. [PubMed: 28439937]
39. Kuehne T, Yilmaz S, Steendijk P, et al. Magnetic resonance imaging analysis of right ventricular pressure-volume loops: in vivo validation and clinical application in patients with pulmonary hypertension. Circulation. 2004; 110, 2010–2016. [PubMed: 15451801]
40. Saba TS, Foster J, Cockburn M, Cowan M, Peacock AJ. Ventricular mass index using magnetic resonance imaging accurately estimates pulmonary artery pressure. Euro Respir J. 2002; 20, 1519–1524.
41. Szczepanska-Sadowska E, Czarzasta K, Cudnoch-Jedrzejewska A. (2018) Dysregulation of the renin-angiotensin system and the vasopressinergic system interactions in cardiovascular disorders. Curr Hypertension Rep. 20, 19.
42. Houben AJ, van der Zander K, de Leeuw PW. Vascular and renal actions of brain natriuretic peptide in man: physiology and pharmacology. Fund Clin Pharm. 2005; 19, 411–419.
43. Perrone-Filardi P, Coca A, Galderisi M, et al. Noninvasive cardiovascular imaging for evaluating subclinical target organ damage in hypertensive patients: a consensus article from the European Association of Cardiovascular Imaging, the European Society of Cardiology Council on Hypertension and the European Society of Hypertension. J Hypertension. 2017; 35, 1727–1741.
44. Hoit BD. Left atrial size and function: role in prognosis. JACC. 2014; 63, 493–505. [PubMed: 24291276]
45. Axel L, Dougherty L. Heart wall motion: improved method of spatial modulation of magnetization for MR imaging. Radiology. 1989; 172, 349–350. [PubMed: 2748813]
46. Kraitchman DL, Young AA, Chang CN, Axel L. Semi-automatic tracking of myocardial motion in MR tagged images. IEEE Trans Med Imag. 1995; 14, 422–433.
47. Schuster A, Hor KN, Kowallick JT, Beerbaum P, Kutty S. Cardiovascular magnetic resonance myocardial feature tracking: concepts and clinical applications. Circ Cardiovasc Imag. 2016; 9, e004077. doi: 10.1161/CIRCIMAGING.115.004077.
48. Barreiro-Pérez M, Curione D, Symons R, Claus P, Voigt JU, Bogaert J. Left ventricular global myocardial strain assessment comparing the reproducibility of four commercially available CMR-feature tracking algorithms. Euro Radiol. 2018; 28, 5137–5147.
49. El Ghannudi S, Germain P, Jeung MY, et al. Discrepancy between regional left ventricular regional circumferential strain assessed by MR-tagging and by speckle tracking echocardiography. J Biomed Graph Comput. 2013; 3, 75–84.
50. Moon JC, Messroghli DR, Kellman P, et al. Myocardial T1 mapping and extracellular volume quantification: a society for cardiovascular magnetic resonance (SCMR) and CMR working group of the European society of cardiology consensus statement. J Cardiovasc Magn Reson. 2013; 15, 92. [PubMed: 24124732]
51. Salemi VM, Rochitte CE, Shiozaki AA, et al. Late gadolinium enhancement magnetic resonance imaging in the diagnosis and prognosis of endomyocardial fibrosis patients. Circ Cardiovasc Imag. 2011; 4(3):304–311.
52. Khalique Z, Ferreira PF, Scott AD, Nielles-Vallespin S, Firmin DN, Pennell DJ. Diffusion tensor cardiovascular magnetic resonance imaging: a clinical perspective. JACC Cardiovasc Imag 2019. doi: 10.1016/j.jcmg.2019.07.016.
53. Guglielmi V, Sbraccia P. Epicardial adipose tissue: at the heart of the obesity complications. Acta Diabet. 2017; 54(9), 805–812.

54. Kuo AH, Li C, Mattern V, Huber HF, et al. Sex-dimorphic acceleration of pericardial, subcutaneous, and plasma lipid increase in offspring of poorly nourished baboons. Intl J Obes. 2018; 42, 1092–1096.
55. Gastl M, Peereboom SM, Gotschy A, et al. Myocardial triglycerides in cardiac amyloidosis assessed by proton cardiovascular magnetic resonance spectroscopy. J Cardiovasc Magn Reson. 2019; 21(1), 10. [PubMed: 30700314]
56. Fillmer A, Hock A, Cameron D, Henning A. Non-water-suppressed 1 H MR spectroscopy with orientational prior knowledge shows potential for separating intra-and extramyocellular lipid signals in human myocardium. Sci Rep. 2017; 7, 1–4. [PubMed: 28127051]
57. Pelc NJ, Herfkens RJ, Shimakawa A, Enzmann DR. Phase contrast cine magnetic resonance imaging. Magn Reson Quart. 1991; 7, 229–254.
58. Hundley WG, Lange RA, Clarke GD, et al. Assessment of coronary arterial flow and flow reserve in humans with magnetic resonance imaging. Circulation. 1996; 93, 1502–1508. [PubMed: 8608617]
59. Sensky PR, Jivan A, Hudson NM, et al. Coronary artery disease: combined stress MR imaging protocol—one-stop evaluation of myocardial perfusion and function. Radiology. 2000; 215, 608–614. [PubMed: 10796946]
60. Markl M, Frydrychowicz A, Kozerke S, Hope M, Wieben O. 4D flow MRI. J Magn Reson Imag. 2012: 36, 1015–1036.
61. Puntmann VO, Valbuena S, Hinojar R, et al. Society for cardiovascular magnetic resonance (SCMR) expert consensus for CMR imaging endpoints in clinical research: part I-analytical validation and clinical qualification. J Cardiovasc Magn Reson. 2018; 20, 1–23. [PubMed: 29298692]
62. Kawel-Boehm N, Maceira A, Valsangiacomo-Buechel ER, et al. Normal values for cardiovascular magnetic resonance in adults and children. J Cardiovasc Magn Reson. 2015; 17, 29. doi: 10.1186/s12968-015-0111-7. [PubMed: 25928314]
63. Petersen SE, Aung N, Sanghvi MM, et al. Reference ranges for cardiac structure and function using cardiovascular magnetic resonance (CMR) in Caucasians from the UK Biobank population cohort. J Cardiovasc Magn Reson. 2017; 19:18. doi: 10.1186/s12968-017-0327-9. [PubMed: 28178995]
64. Le Ven F, Bibeau K, De Larochellière É, et al. Cardiac morphology and function reference values derived from a large subset of healthy young Caucasian adults by magnetic resonance imaging. Eur Heart J Cardiovasc Imaging. 2016; 17, 981–990. [PubMed: 26354980]
65. Maceira AM, Cosin-Sales J, Prasad SK, Pennell DJ. Characterization of left and right atrial function in healthy volunteers by cardiovascular magnetic resonance. J Cardiovasc Magn Reson. 2016; 18, 64. doi: 10.1186/s12968-016-0284-8. [PubMed: 27719670]
66. Sarikouch S, Peters B, Gutberlet M, et al. Sex-specific pediatric percentiles for ventricular size and mass as reference values for cardiac MRI: assessment by steady-state free-precession and phase-contrast MRI flow. Circ Cardiovasc Imaging. 2010; 3, 65–76. [PubMed: 19820203]
67. Sarikouch S, Koerperich H, Boethig D, et al. Reference values for atrial size and function in children and young adults by cardiac MR: a study of the German competence network congenital heart defects. J Magn Reason Imag. 2011; 33, 1028–1039.
68. Natori S, Lai S, Finn JP, Gomes AS, et al. Cardiovascular function in multiethnic study of atherosclerosis: normal values by age, sex, and ethnicity. AJR Am J Roentgenol. 2006; 186, S357–S365. [PubMed: 16714609]
69. Zemrak F, Ambale-Venkatesh B, Captur G, et al. Left atrial structure in relationship to age, sex, ethnicity, and cardiovascular risk factors: MESA (Multi-ethnic study of atherosclerosis). Circ Cardiovasc Imaging. 2017; 10, e005379. doi: 10.1161/CIRCIMAGING.116.005379.. [PubMed: 28196797]
70. Le TT, San Tan R, De Deyn M, et al. Cardiovascular magnetic resonance reference ranges for the heart and aorta in Chinese at 3T. J Cardiovasc Magn Reson. 2016; 18, 21. doi: 10.1186/s12968-016-0236. [PubMed: 27071974]
71. Kim PK, Hong YJ, Im DJ, et al. Myocardial T1 and T2 mapping: techniques and clinical applications. Korean J Radiol. 2017; 18, 113–131. [PubMed: 28096723]

72. Lee JJ, Liu S, Nacif MS, et al. Myocardial T1 and extracellular volume fraction mapping at 3 tesla. J Cardiovasc Magn Reson. 2011; 13, 75. doi: 10.1186/1532-429X-13-75. [PubMed: 22123333]
73. Roy C, Slimani A, de Meester C, et al. Age and sex corrected normal reference values of T1, T2 T2* and ECV in healthy subjects at 3T CMR. J Cardiovasc Magn Reson. 2017; 19, 72. doi: 10.1186/s12968-017-0371-5. [PubMed: 28934962]
74. Barczuk-Falęcka M, Małek ŁA, Werys K, Roik D, Adamus K, Brzewski M. (2020) Normal values of native T1 and T2 relaxation times on 3T cardiac MRin a healthy pediatric population aged 9–18 years. J Magn Reson Imag. 51, 912–918.
75. Burkhardt BE, Menghini C, Rücker B, Kellenberger CJ, Valsangiacomo Buechel ER. Normal myocardial native T1 values in children using single-point saturation recovery and modified look–locker inversion recovery (MOLLI). J Magn Reason Imag. 2020; 51, 897–903.
76. Dabir D, Child N, Kalra A, et al. Reference values for healthy human myocardium using a T1 mapping methodology: results from the International T1 Multicenter cardiovascular magnetic resonance study. J Cardiovasc Magn Reson. 2014; 16, 69. doi: 10.1186/s12968-014-0069-x. [PubMed: 25384607]
77. Magri D, Sciomer S, Fedele F, et al. Early impairment of myocardial function in young patients with β-thalassemia major. Eur J Haematol. 2008; 80, 515–522. [PubMed: 18284626]
78. Boss A, Oppitz M, Wehrl HF, et al. Measurement of T1, T2, and magnetization transfer properties during embryonic development at 7 Tesla using the chicken model. J Magn Reson Imag. 2008; 28, 1510–1514.
79. Broadhouse KM, Finnemore AE, Price AN, et al. Cardiovascular magnetic resonance of cardiac function and myocardial mass in preterm infants: a preliminary study of the impact of patent ductus arteriosus. J Cardiovasc Magn Reson. 2014; 16, 54. [PubMed: 25160730]
80. Toemen L, Jelic G, Kooijman MN, et al. Third trimester fetal cardiac blood flow and cardiac outcomes in school-age children assessed by magnetic resonance imaging. J Am Heart Assoc. 2019; 8, e012821. doi: 10.1161/JAHA.119.01282. [PubMed: 31405324]
81. Groves AM, Chiesa G, Durighel G, et al. Functional cardiac MRI in preterm and term newborns. Arch Dis Child Fetal Neonatal Ed. 2011; 96, F86–F91. [PubMed: 20971721]
82. Poon CY, Edwards JM, Evans CJ, et al. Assessment of pulmonary artery pulse wave velocity in children: an MRI pilot study. Magn Reson Imag. 2013; 31, 1690–1694.
83. André F, Robbers-Visser D, Helling-Bakki A, et al. Quantification of myocardial deformation in children by cardiovascular magnetic resonance feature tracking: determination of reference values for left ventricular strain and strain rate. J Cardiovasc Magn Reson. 2017; 19, 8. doi: 10.1186/s12968-016-0310-x.
84. Roy CW, Marini D, Seed M, Macgowan CK. Fetal Cardiac MRI: a review of technical advancements. Top Magn Reason Imag. 2019; 28, 235–244.
85. Cho SK, Darby JR, Saini BS, et al. Feasibility of ventricular volumetry by cardiovascular MRI to assess cardiac function in the fetal sheep. J Physiol. 2020; 598, 2557–2573. [PubMed: 32378201]
86. Roberts TA, van Amerom JF, Uus A, et al. Fetal whole heart blood flow imaging using 4D cine MRI. Nat Commun. 2020; 11, 1–3. [PubMed: 31911652]
87. Schrauben EM, Saini BS, Darby JR, et al. Fetal hemodynamics and cardiac streaming assessed by 4D flow cardiovascular magnetic resonance in fetal sheep. J Cardiovasc Magn Reson. 2019; 21, 8. [PubMed: 30661506]
88. Saini BS, Darby JR, Portnoy S, et al. Normal human and sheep fetal vessel oxygen saturations by T2 magnetic resonance imaging. J Physiol. 2020; 598, 3259–3281. [PubMed: 32372463]
89. Zhu MY, Milligan N, Keating S, et al. The hemodynamics of late-onset intrauterine growth restriction by MRI. Am J Obstet Gynecol. 2016; 214, 367.e1–367.e17. doi: 10.1016/j.ajog.2015.10.004. [PubMed: 26475425]
90. Toemen L, Gaillard R, Roest AA, et al. Fetal and infant growth patterns and left and right ventricular measures in childhood assessed by cardiac MRI. Eur J Prev Cardiol. 2019. doi: 10.1177/2047487319866022.
91. Kingdom T, Zhu MY, Porayette P, et al. The absolute and relative sizes of the brains and bodies of fetuses with different forms of congenital heart disease and intrauterine growth restriction. J Cardiovasc Magn Reson. 2016; 18. doi: 10.1186/1532-429X-18-S1-P151.

92. Cohn HE, Sacks EJ, Heymann MA, Rudolph AM. Cardiovascular responses to hypoxemia and acidemia in fetal lambs. Obstet Gynecol. 1974; 120, 817–824.

93. Cox DJ, Bai W, Price AN, Edwards AD, Rueckert D, Groves AM. Ventricular remodeling in preterm infants: computational cardiac magnetic resonance atlasing shows significant early remodeling of the left ventricle. Pediatr Res. 2019; 85, 807–815. [PubMed: 30758323]

94. Rabadan-Diehl C, Nathanielsz P. From Mice to men: research models of developmental programming. J Dev Origins Health Dis. 2013; 4, 3–9.

95. Schlabritz-Loutsevitch NE, Howell K, Rice K, et al. Development of a system for individual feeding of baboons maintained in an outdoor group social environment. J Med Primatol. 2004; 33, 117–126. [PubMed: 15102068]

96. Kuo AH, Li C, Li J, Huber HF, Nathanielsz PW, Clarke GD. Cardiac remodeling in a baboon model of intrauterine growth restriction mimics accelerated ageing. J Physiol. 2017; 595, 1093–1110. [PubMed: 27988927]

97. Rozance PJ, Seedorf GJ, Brown A, et al. Intrauterine growth restriction decreases pulmonary alveolar and vessel growth and causes pulmonary artery endothelial cell dysfunction in vitro in fetal sheep. Am J Physio Lung Cell Mol Physiol. 2011; 301: L860–L871.

98. Kuo AH, Li J, Li C, Huber HF, Nathanielsz PW, Clarke GD. Poor perinatal growth impairs baboon aortic windkessel function. J Dev Orig Health Dis. 2018; 9, 137–142. [PubMed: 29017630]

99. Kuo AH, Li C, Huber HF, Clarke GD, Nathanielsz PW. Intrauterine growth restriction results in persistent vascular mismatch in adulthood. J Physiol. 2018; 596, 5777–5790. [PubMed: 29098705]

100. Corstius HB, Zimanyi MA, Maka N, et al. Effect of intrauterine growth restriction on the number of cardiomyocytes in rat hearts. Pediatr Res. 2005; 57, 796–800. [PubMed: 15774830]

101. Botting KJ, McMillen IC, Forbes H, Nyengaard JR, Morrison JL. Chronic hypoxemia in late gestation decreases cardiomyocyte number but does not change expression of hypoxia-responsive genes. J Am Heart Assoc. 2014; 3(4), e000531. [PubMed: 25085511]

102. Morrison JL, Botting KJ, Dyer JL, Williams SJ, Thornburg KL, McMillen IC. Restriction of placental function alters heart development in the sheep fetus. Am J Physiol Regul Integr Comp Physiol. 2007; 293, R306–R313. [PubMed: 17428893]

103. Bubb KJ, Cock ML, Black MJ, et al. Intrauterine growth restriction delays cardiomyocyte maturation and alters coronary artery function in the fetal sheep. J Physiol (Lond). 2007; 578, 871–881. [PubMed: 17124269]

104. Harvey TJ, Murphy RM, Morrison JL, Posterino GS. Maternal nutrient restriction alters Ca2 handling properties and contractile function of isolated left ventricle bundles in male but not female juvenile rats. PLoS One. 2015; 10, e0138388. [PubMed: 26406887]

105. Iruretagoyena JI, Gonzalez-Tendero A, Garcia-Canadilla P, et al. Cardiac dysfunction is associated with altered sarcomere ultrastructure in intrauterine growth restriction. Obstet Gynecol. 2014; 210, 550.e1–550.e7.

106. Bezerra DG, Andrade LML, da Cruz FOP, Mandarim-de-Lacerda CA. Atorvastatin attenuates cardiomyocyte loss in adult rats from protein-restricted dams. J Card Fail. 2008; 14, 151–160. [PubMed: 18325463]

107. Nakamori S, Dohi K, Ishida M, et al. Native T1 mapping and extracellular volume mapping for the assessment of diffuse myocardial fibrosis in dilated cardiomyopathy. JACC Cardiovasc Imag. 2018; 11, 48–59.

108. Enriquez-Sarano M, Rossi A, Seward JB, Bailey KR, Tajik AJ. Determinants of pulmonary hypertension in left ventricular dysfunction. J Am Coll Cardiol. 1997; 29, 153–159. [PubMed: 8996308]

109. Thompson JA, Gros R, Richardson BS, Piorkowska K, Regnault TR. Central stiffening in adulthood linked to aberrant aortic remodeling under suboptimal intrauterine conditions. Am J Physiol Regul Integr Comp Physiol. 2011; 301, 1731–1737.

110. Khorram O, Momeni M, Desai M, Ross MG. Nutrient restriction in utero induces remodeling of the vascular extracellular matrix in rat offspring. Reprod Sci. 2007; 14(1), 73–80. [PubMed: 17636219]

111. Dodson RB, Rozance PJ, Petrash CC, Hunter KS, Ferguson VL. Thoracic and abdominal aortas stiffen through unique extracellular matrix changes in intrauterine growth restricted fetal sheep. Am J Physiol Heart Circ Physiol. 2014; 306, H429–H437. [PubMed: 24322609]
112. Strait JB, Lakatta EG. Aging-associated cardiovascular changes and their relationship to heart failure. Heart Fail Clin. 2012; 8, 143–164. [PubMed: 22108734]
113. Sampath S, Parimal AS, Feng D, et al. Quantitative MRI biomarkers to characterize regional left ventricular perfusion and function in nonhuman primates during dobutamine-induced stress: a reproducibility and reliability study. J Magn Reson Imag. 2017; 45, 556–569.
114. Pashakhanloo F, Herzka DA, Ashikaga H, et al. Myofiber architecture of the human atria as revealed by submillimeter diffusion tensor imaging. Circ Arrhythm Electrophysiol. 2016; 9, e004133. [PubMed: 27071829]
115. Mekkaoui C, Reese TG, Jackowski MP, Bhat H, Sosnovik DE. Diffusion MRI in the heart. NMR Biomed. 2017; 30, e3426.
116. Darby JR, McMillen IC, Morrison JL. Maternal undernutrition in late gestation increases IGF2 signaling molecules and collagen deposition in the right ventricle of the fetal sheep heart. J Physiol. 2018; 596, 2345–2358. [PubMed: 29604078]
117. Ohno Y, Hatabu H, Murase K, et al. Primary pulmonary hypertension: 3D dynamic perfusion MRI for quantitative analysis of regional pulmonary perfusion. Am J Roentgenol. 2007; 188, 48–56. [PubMed: 17179345]
118. Clarke GD, Eckels R, Chaney C, et al. Measurement of absolute epicardial coronary artery flow and flow reserve using breath-hold cine phase-contrast magnetic resonance imaging. Circulation. 1995; 91, 2627–2634. [PubMed: 7743626]
119. Guensch DP, Friedrich MG. Novel approaches to myocardial perfusion: 3D first-pass CMR perfusion imaging and oxygenation-sensitive CMR. Curr Cardiovasc Imaging Rep. 2014; 7, 9261.
120. Cox LA, Nijland MJ, Gilbert JS, et al. Effect of 30 per cent maternal nutrient restriction from 0.16 to 0.5 gestation on fetal baboon kidney gene expression. J Physiol. 2006; 572, 67–85. [PubMed: 16513668]
121. Zhang JL, Lee VS. Renal perfusion imaging by MRI. J MAGN Reson Imag. 2020; 52, 369–379.
122. Khatir DS, Pedersen M, Jespersen B, Buus NH. Evaluation of renal blood flow and oxygenation in CKD using magnetic resonance imaging. Am J Kid Dis. 2015; 66, 402–411. [PubMed: 25618188]
123. Collinot H, Marchiol C, Lagoutte I, et al. Preeclampsia induced by STOX1 overexpression in mice induces intrauterine growth restriction, abnormal ultrasonography and BOLD MRI signatures. J Hypertension. 2018; 36, 1399–1406.
124. Catalano PM, Presley L, Minium J, Hauguel-de Mouzon S. Fetuses of obese mothers develop insulin resistance in utero. Diabetes Care. 2009; 32, 1076–1080. [PubMed: 19460915]
125. Choi J, Li C, McDonald TJ, Comuzzie A, Mattern V, Nathanielsz PW. Emergence of insulin resistance in juvenile baboon offspring of mothers exposed to moderate maternal nutrient reduction. Am J Physiol Reg Integr Comp Physiol. 2011; 301, R757–R762.
126. Reingold JS, McGavock JM, Kaka S, Tillery T, Victor RG, Szczepaniak LS. Determination of triglyceride in the human myocardium by magnetic resonance spectroscopy: reproducibility and sensitivity of the method. Am J Physiol Endo Metab. 2005; 289, E935–E939.
127. Holloway CJ, Cochlin LE, Emmanuel Y, et al. A high-fat diet impairs cardiac high-energy phosphate metabolism and cognitive function in healthy human subjects. Am J Clin Nutr. 2011; 93, 748–755. [PubMed: 21270386]
128. Somerville LH, Bookheimer SY, Buckner RL, et al. The lifespan human connectome project in development: a large-scale study of brain connectivity development in 5–21 year olds. Neuroimage. 2018; 183, 456–468. [PubMed: 30142446]
129. Arthurs OJ, Rega A, Guimiot F, et al. Diffusion-weighted magnetic resonance imaging of the fetal brain in intrauterine growth restriction. Ultrasound Obst Gyn. 2017; 50, 79–87.
130. Polat A, Barlow S, Ber R, Achiron R, Katorza E. Volumetric MRI study of the intrauterine growth restriction fetal brain. Euro Radiol. 2017; 27, 2110–2118.

131. Andersson C, Johnson AD, Benjamin EJ, Levy D, Vasan RS. 70-year legacy of the Framingham Heart Study. Nat Rev Cardiol. 2019; 16, 687. [PubMed: 31065045]

132. Hooghiemstra AM, Bertens AS, Leeuwis AE, et al. The missing link in the pathophysiology of vascular cognitive impairment: design of the Heart-Brain Study. Cerebrovasc Dis Extra. 2017; 7, 140–152. [PubMed: 29017156]

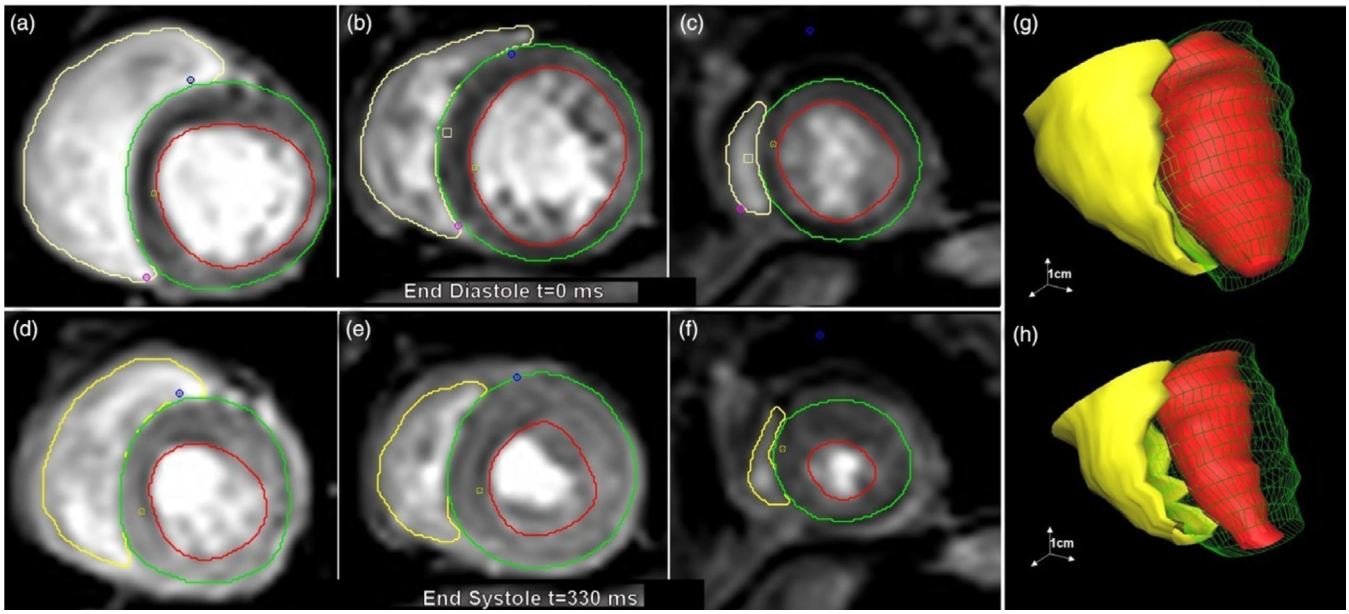

Fig. 1.

Selection of left ventricular (LV) subendocardial margin (red lines), LV subepicardial margin (green lines), and right ventricular (RV) subendocardial margin (yellow lines) is performed manually or semi-automatically for up to 20 slices. Typical basal slice (a), midventricular slice (b), and apical slice (c) are shown at end-diastole (ED). Basal slice (d), midventricular (e), and apical slices (f) are also determined at end-systole (ES) and at 25–30 cardiac phases in between. From these data, full RV and LV volumes can be reconstructed at ED (g) and ES (h).

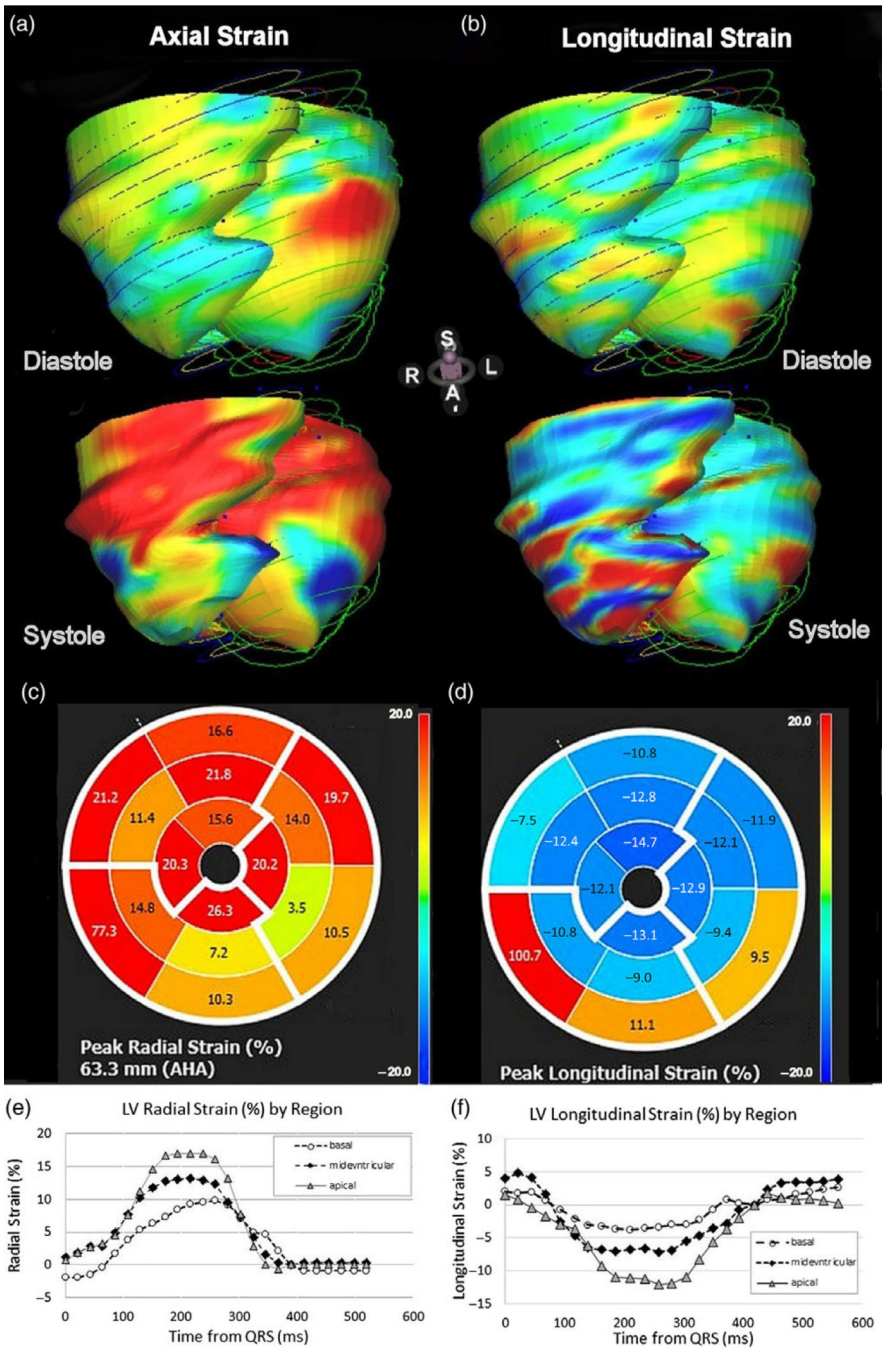

Fig. 2.

Examples of parametric strain images calculated using MR feature tracking from breath-hold cine acquisitions (a) axial and (b) longitudinal strain surface coding for diastolic (top) and systolic (bottom) phases. Middle insert shows polar plots of maximal strain in the axial (c) and longitudinal directions (d). Plots of radial strain (e) and longitudinal strain over the cardiac cycle shows greater strains in both directions in the apical region of the baboon heart.

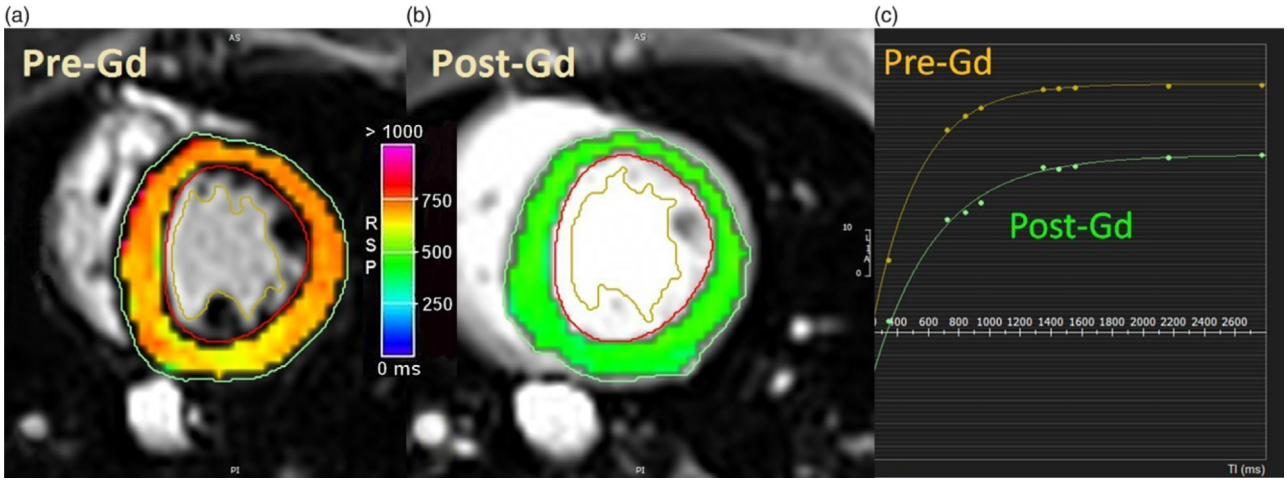

Fig. 3.

Parametric maps of the *T*1 of the baboon left ventricle in short-axis views. (a) *T*1 parametric map of native myocardium. (b) *T*1 parametric map of myocardium ~10 min after gadolinium (Gd) administration. Note the GD reduces *T*1. (c) *T*1 measurement requires acquiring several images with different timing intervals. *T*1 recovery curves were generated for nine images taken at different timings. Circumferential strain, not shown, can also be calculated and displayed in a similar fashion.

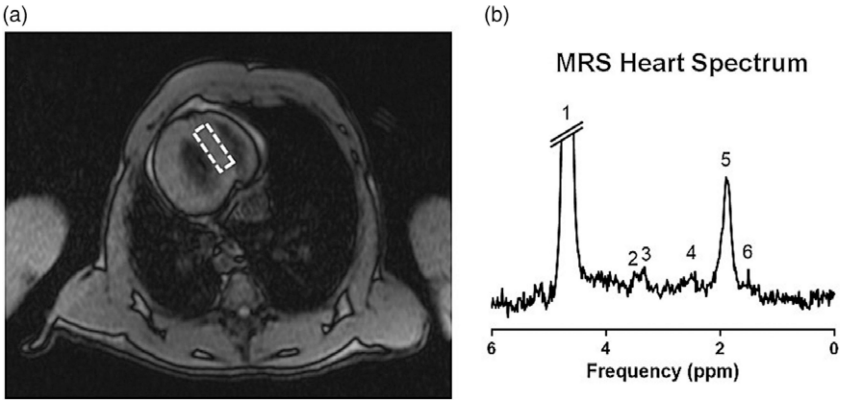

Fig. 4.

Example of a hydrogen-1 magnetic resonance spectrum (1 H-MRS) from a baboon heart. (a) Scout image is used to define the position in the interventricular septum (dashed rectangle) from which the 1 H-MRS data is sampled. (b) Sample spectrum from a prior study identifying six major resonances, including three peaks of triglyceride (4, 5, and 6) and single peaks of creatine (3), trimethyl-ammonium compounds (2), and water (1).

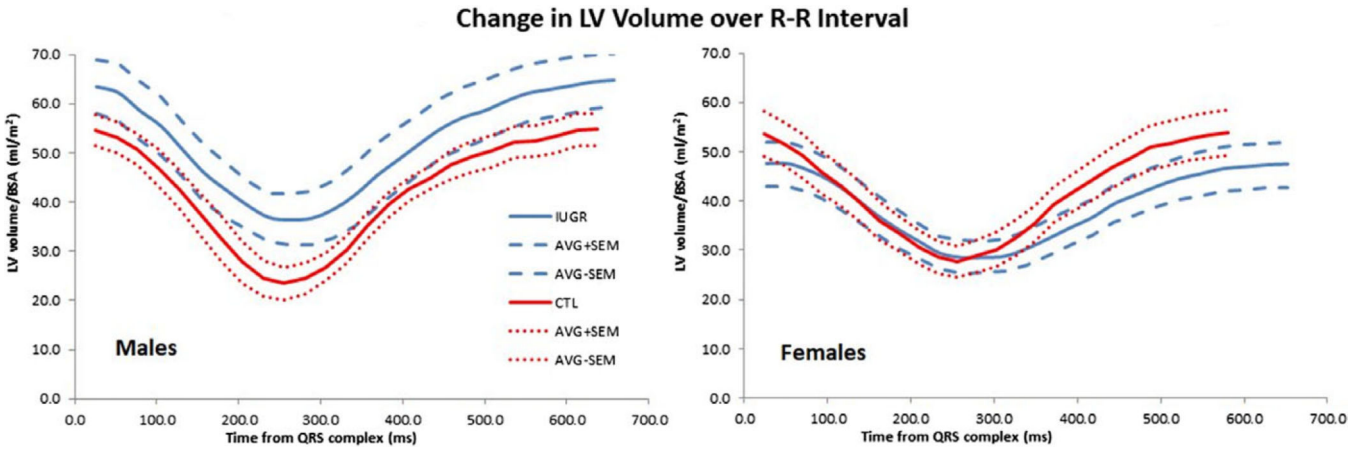

Fig. 5.

Sex differences were found in normalized LV time–volume curves across the cardiac cycle. Right for IUGR male baboons (blue lines), LV volumes tend to increase relative to control animals (red lines). Left for females, LV volumes tend to decrease in IUGR relative to younger subjects. Resting heart rate for IUGR animals is slower for both sexes. Data represent average normalized LV volume (continuous lines) and mean ± SEM (dashed lines) for animals, and are described in Ref. 96.

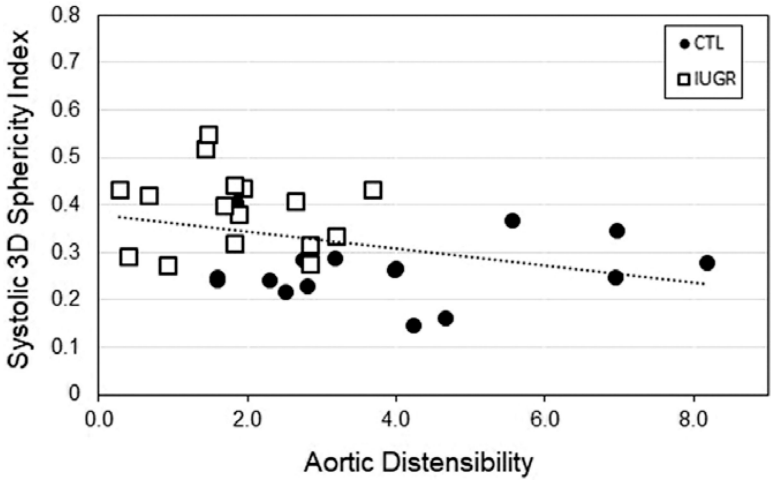

Fig. 6.

Data are from 16 controls (8M/8 F), open boxes, and 16 IUGR (8M/8 F) baboons, black circles. Three-dimensional (3D) sphericity index is negatively correlated with aortic distensibility in the baboon ($r = -0.36$, $p = 0.04$). Increasing LV sphericity is an index of ventricular remodeling.

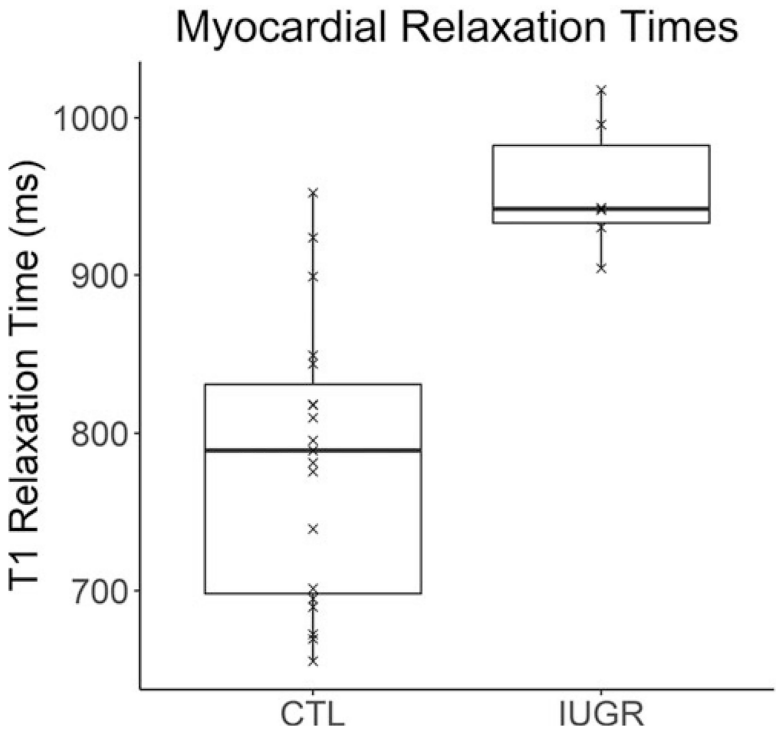

Fig. 7.

Significant increase ($p = 0.001$) of native myocardial $T1$ values was measured in IUGR compared to control (CTL) group ($n = 19$, M/F = 8/11, age = 6.1 + 1.3 years.) versus IUGR group ($n = 6$, M/F = 2/4, age = 4.8 + 0.5 years.). $T1$ is indicative of higher myocardial collagen content even though control group is, on average, slightly older than IUGR group. Solid line = median; box covers interquartile range; whiskers cover full data range.

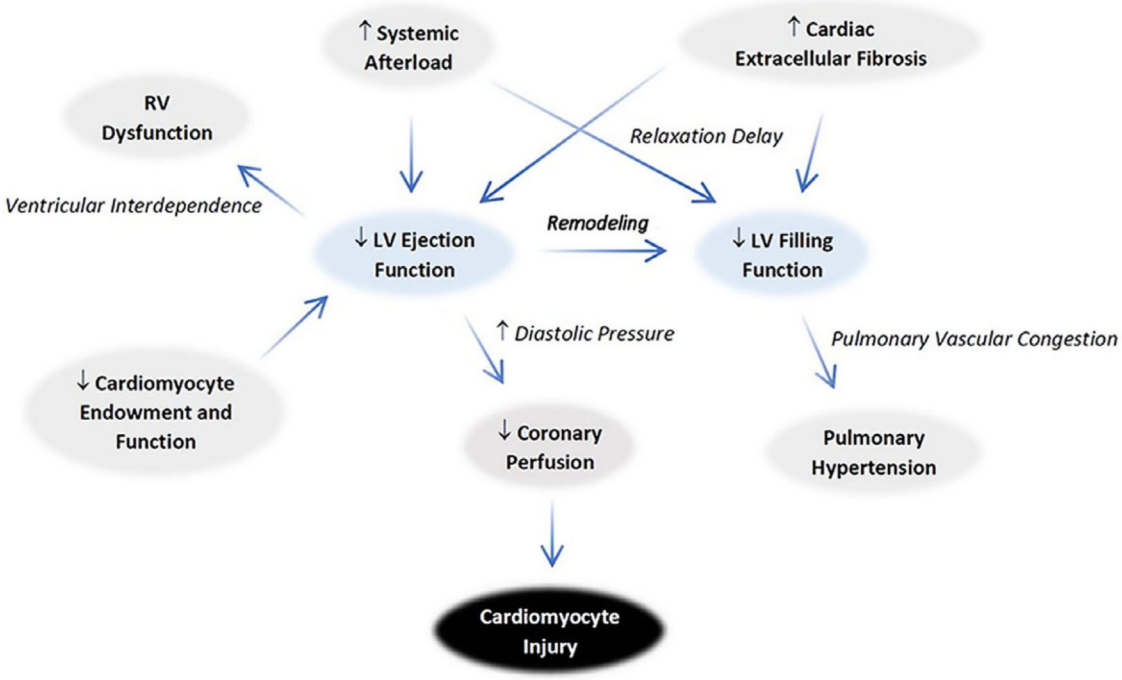

Fig. 8.

Proposed mechanisms for IUGR cardiac pathophysiology. An overall congestive physiology is evidenced by the ventricular remodeling that increases sphericity in both systole and diastole. The decrease in ejection fraction worsens filling dysfunction via an increase in diastolic pressure. The RV changes mirror the left in many regards. The increase in diastolic pressure contributes to decreased coronary perfusion, which predisposes to cardiomyocyte injury. The pattern of ventricular changes raises concerns that afterload increases as well.

Table 1.

CMR quantitative endpoints and relative accuracy [after Puntmann, 2018]

Class of measurement	Parameter(s) measured	Analytical validation	Precision	Additional comments
Ventricular volumes and function	LV and RV volumes, EF, aortic pulse waveform	Excellent validation	Inter-study, inter- and intra-observer reproducibility	Reference standard for LV and RV volume, function, and mass quantitation.
Regional wall motion and deformation	Longitudinal and Circumferential strains	Well validated	Limited data on interstudy reproducibility	Similar to echo for assessing longitudinal motion and strain
Diastolic function	E/A waveform, ventricular filling rate	Validated versus PV loops and echo		Diastolic filling, atrial function, trans-mitral and pulmonary flow
Myocardial tissue characterization	*T*1 parametric maps	Validated in phantoms, animal models, human biopsies, and explanted hearts	Evidence available on inter-study, inter- and intra-observer variability	Predictors of nonischemic dilated cardiomyopathy outcomes. Sequence-specific normal values are available.
	*T*2 parametric maps	Validated versus phantoms, animal models, biopsies, and other imaging biomarkers		Useful in detecting myocardial edema and inflammation. Sequence-specific normal values are available
	*T*2* parametric maps	Excellently validated and standardized in iron-overload	Evidence on inter-scanner, inter-center, inter-study, inter- and intra-observer variability	Outcome data in thalassemia major. Prognostic information after a coronary event. Normal values and established clinically relevant cut-offs available
Vascular	Structure	Limited reproducibility evidence of tissue measurements	Normal values available for different anatomical and functional measurements	Aortic and carotid vessel wall imaging, are robust markers of atherosclerotic burden
	Function	Excellent evidence for PWV.		PWV: pulse wave velocity
Myocardial Perfusion	Evidence for visual detection of ischemia is favorable. Quantification promising.	Limited evidence on inter-study, inter,- and intra-observer reproducibility due to need for stress and contrast injection		First-line technique for assessing the presence, extent, and localization of inducible ischemia. Limited data on normal values due to the lack of standardization.

J Dev Orig Health Dis. Author manuscript; available in PMC 2021 October 01.

Table 2.

Normative reference ranges for human left ventricular (LV) function by age

Age group (years)	8–15[§]	16–20[§]	18–35[**]	45–54[*]	55–64[*]	65–74[*]
Male						
LVEDV/BSA (ml/m^2)	81.9 ± 12.9	93.5 ± 10.9	89 ± 13	86 (60–122)	86 (55–117)	81 (52–110)
LVESV/BSA (ml/m^2)	28.2 ± 6.7	35.9 ± 7.1	31 ± 7	36 (21–51)	36 (20–52)	34 1(9–49)
LVSV/BSA (ml/m^2)	53.7 ± 8.5	57.6 ± 5.9	58 ± 8	50 (32–68)	50 (30–70)	47 (28–67)
LV mass/BSA (g/m^2)	52.1 ± 10.6	67.6 ± 7.7	64 ± 11	54 (35–72)	53 (34–72)	51 (33–70)
LVEF (%)	65.7 ± 4.9	61.8 ± 4.3	65 ± 5	58 (47–70)	58 (48–69)	58 (47–69)
LV mass/volume (g/ml)	NA	NA	0.73 ± 0.1	0.63 (0.42–0.84)	0.62 (0.4–0.85)	0.64 (0.41–0.87)
Female						
LVEDV/BSA (ml/m^2)	78.7 ± 10.7	80.7 ± 9.5	77 ± 8	78 (54–101)	72 (50–94)	73 (50–96)
LVESV/BSA (ml/m^2)	28.9 ± 6.1	29.0 ± 7.5	26 ± 5	31 (19–43)	28 (16–40)	29 (16–42)
LVSV/BSA (ml/m^2)	49.7 ± 8.3	51.7 ± 5.9	51 ± 6	47 (30–63)	44 (29–59)	45 (29–60)
LV mass/BSA (g/m^2)	48.2 ± 8.2	51.2 ± 7.3	49 ± 8	42 (29–55)	41 (28–55)	42 (28–55)
LVEF (%)	63.2 ± 6.3	61.8 ± 4.3	65 ± 5	60 (50–70)	61 (51–72)	61 (50–72)
LV mass/volume (g/ml)	NA	NA	0.64 ± 0.1	0.55 (0.39–0.71)	0.58 (0.36–0.8)	0.58 (0.35–0.81)

NA, not available.

[*] Petersen, 2017 (variability given as prediction interval).

[**] Le Ven, 2016.

[§] Sarikouch, 2010 (variability given as +SD).

Table 3.

Normative reference ranges for human right ventricular (RV) function by age

Age group (years)	8–15[§]	16–20[§]	18–35[**]	45–54[*]	55–64[*]	65–74[*]
Male						
RVEDV/BSA (ml/m^2)	82.9 ± 12.6	90.2 ± 10.9	101 ± 26	97 (68–126)	92 (56–128)	90 (55–125)
RVESV/BSA (ml/m^2)	31.3 ± 6.1	36.1 ± 6.3	39 ± 9	46 (25–67)	42 (21–63)	42 (19–66)
RVSV/BSA (ml/m^2)	51.6 ± 8.4	54.1 ± 7.3	62 ± 12	51 (34–68)	50 (31–69)	48 (30–67)
RV mass/BSA (g/m^2)	18.3 ± 5.5	26.9 ± 2.7	NA	NA	NA	NA
RVEF (%)	62.3 ± 4.3	60.0 ± 4.4	62 ± 7	53 (40–65)	55 (45–65)	54 (40–68)
Female						
RVEDV/BSA (ml/m^2)	82.9 ± 12.6	90.2 ± 10.9	101 ± 26	81 (53–1110)	75 (51–99)	77 (53–101)
RVESV/BSA (ml/m^2)	31.3 ± 6.1	36.1 ± 6.3	39 ± 9	36 (17–55)	31 (16–46)	32 (17–48)
RVSV/BSA (ml/m^2)	51.6 ± 8.4	54.1 ± 7.3	62 ± 12	46 (30–61)	44 (29–59)	44 (30–59)
RV mass/BSA (g/m^2)	18.3 ± 5.5	26.9 ± 2.7	NA	NA	NA	NA
RVEF (%)	62.3 ± 4.3	60.0 ± 4.4	62 ± 7	56 (45–68)	59 (47–70)	58 (46–70)

NA, not available.

[*] Petersen, 2017 (variability given as prediction interval).

[**] Le Ven, 2016.

[§] Sarikouch, 2010 (variability given as +SD).

Table 4.

Normative reference ranges for human left atrial (LA) function by age

Age group (years)	5–20[§]	18–35[**]	45–54[*]	55–64[*]	65–74[*]
Male					
Max LA volume/BSA (ml/m^2)	46.7 ± 10.1	41 ± 8	37 (18–56)	37 (19–55)	35 (15–55)
Min LA volume/BSA (ml/m^2)	21.5 ± 5.1	17 ± 4	NA	NA	NA
LA SV/BSA (ml/m^2)	NA	24 ± 6	22 (11–33)	22 (12–33)	21 (9–32)
LA EF (%)	53.7 ± 6.3	59 ± 8	59 (45–73)	61 (47–75)	59 (44–74)
Female					
Max LA volume/BSA (ml/m^2)	44.2 ± 8.7	38 ± 7	39 (21–57)	36 (16–56)	36 (18–55)
Min LA volume/BSA (ml/m^2)	19.2 ± 3.9	15 ± 4	NA	NA	NA
LA SV/BSA (ml/m^2)	NA	24 ± 5	24 (13–34)	22 (10–23)	21 (11–32)
LA EF (%)	56.2 ± 5.5	61 ± 7	62 (49–75)	61 (44–77)	59 (45–74)

NA, not available.

[*] Petersen, 2017 (variability given as prediction interval).

[**] Le Ven, 2016.

[§] Sarikouch, 2011 (variability given as +SD).

Table 5.

Normative values for relaxation time in healthy human myocardium by age groups

Age group (years)	8–18[§] 9–18[‡]	<30[*] 20–30[**]	31–42[*] 30–40[**]	42–53[*] 40–50[**]	>53[*] 50–60[**]	60–70[**]	70–80[**]	>80[**]
Myocardial *T*1 @1.5 T (ms)	1010 ± 48[§]	952 ± 22[*]	953 ± 25[*]	957 ± 25[*]	NA	NA	NA	NA
Myocardial *T*1 @ 3.0 T (ms)	1223 ± 29[‡]	1053 ± 26[*] 1070 ± 80[**]	1057 ± 24[*] 1114 ± 43[**]	1058 ± 25[*] 1100 ± 54[**]	1052 ± 24[*] 1132 ± 42[**]	1144+51[**]	1141 ± 42[**]	1142 ± 64[**]
Myocardial *T*2 (ms)	43 ± 4.5[‡]	53 ± 5[**]	52 ± 4[**]	53 ± 4[**]	55 ± 2[**]	53 ± 7[**]	52 ± 6[**]	43 ± 5[**]
Myocardial $T2^*$ (ms)	NA	23 ± 5[**]	26 ± 5[**]	21 ± 6[**]	21 ± 6[**]	24 ± 3[**]	25 ± 5[**]	28 ± 3[**]

NA, not available.

[§]Burkhardt, 2020.

[‡]Barczuk-Falęcka, 2020.

[*]Dabir, 2014.

[**]Roy, 2017.